Plant Communications
Research article

CellPress
Partner Journal

MYB44 regulates PTI by promoting the expression of *EIN2* and *MPK3/6* in *Arabidopsis*

Zuodong Wang[1,5], Xiaoxu Li[1,5], Xiaohui Yao[1,4,5], Jinbiao Ma[3], Kai Lu[1], Yuyan An[2], Zhimao Sun[2], Qian Wang[1], Miao Zhou[1], Lina Qin[1], Liyuan Zhang[1], Shenshen Zou[1], Lei Chen[1], Congfeng Song[3], Hansong Dong[1,4,*], Meixiang Zhang[2,*] and Xiaochen Chen[1,*]

[1]College of Plant Protection, Shandong Agricultural University, Taian 271018, China

[2]College of Life Sciences, Shaanxi Normal University, Xi'an 710119, China

[3]College of Plant Protection, Nanjing Agricultural University, Nanjing 210095, China

[4]Qilu College, Shandong Agricultural University, Taian 271018, China

[5]These authors contributed equally to this article.

***Correspondence: Hansong Dong (hsdong@sdau.edu.cn), Meixiang Zhang (meixiangzhang@snnu.edu.cn), Xiaochen Chen (chenxc66@sdau.edu.cn)**

https://doi.org/10.1016/j.xplc.2023.100628

ABSTRACT

The plant signaling pathway that regulates pathogen-associated molecular pattern (PAMP)-triggered immunity (PTI) involves mitogen-activated protein kinase (MAPK) cascades that comprise sequential activation of several protein kinases and the ensuing phosphorylation of MAPKs, which activate transcription factors (TFs) to promote downstream defense responses. To identify plant TFs that regulate *MAPK*s, we investigated TF-defective mutants of *Arabidopsis thaliana* and identified MYB44 as an essential constituent of the PTI pathway. MYB44 confers resistance against the bacterial pathogen *Pseudomonas syringae* by cooperating with MPK3 and MPK6. Under PAMP treatment, MYB44 binds to the promoters of *MPK3* and *MPK6* to activate their expression, leading to phosphorylation of MPK3 and MPK6 proteins. In turn, phosphorylated MPK3 and MPK6 phosphorylate MYB44 in a functionally redundant manner, thus enabling MYB44 to activate *MPK3* and *MPK6* expression and further activate downstream defense responses. Activation of defense responses has also been attributed to activation of *EIN2* transcription by MYB44, which has previously been shown to affect PAMP recognition and PTI development. AtMYB44 thus functions as an integral component of the PTI pathway by connecting transcriptional and posttranscriptional regulation of the MPK3/6 cascade.

Key words: *Arabidopsis*, MPK cascade, MPK3/6, EIN2, MYB44, PTI

Wang Z., Li X., Yao X., Ma J., Lu K., An Y., Sun Z., Wang Q., Zhou M., Qin L., Zhang L., Zou S., Chen L., Song C., Dong H., Zhang M., and Chen X. (2023). MYB44 regulates PTI by promoting the expression of *EIN2* and *MPK3/6* in *Arabidopsis*. Plant Comm. **4**, 100628.

INTRODUCTION

Plants deploy multiple arrays of immunity to defend themselves against pathogen attacks, while prioritizing pathogen-associated molecular pattern (PAMP)-triggered immunity (PTI) as the battlefront (Zipfel et al., 2004; Zhang and Zhou, 2010; Zhang et al., 2020). PTI is activated by molecular interactions between PAMPs (Asai et al., 2002; Asai et al., 2002) and pattern recognition receptors (PRRs) located in the plasma membranes (PMs) of plant cells (Zipfel et al., 2006; Zipfel, 2014; Tian et al., 2021; Schulze et al., 2022). Typical PRRs are receptor-like kinases that possess an extracellular ligand-binding domain to perceive signal inputs, a single transmembrane domain to anchor the kinase protein in the PM, and an intracellular kinase domain essential for signal transduction via kinase cascades (Gómez-Gómez and Boller, 2000; Asai et al., 2002; Zipfel, 2014). PRRs directly interact with PAMPs via the ligand-binding domain to form heterogeneous protein complexes called PAMP-PRRs (Dunning et al., 2007; Kanyuka and Rudd, 2019). PAMP-PRRs then bind to a different receptor-like kinase to trigger mitogen-activated protein kinase (MAPK) cascades, which comprise sequential phosphorylation and activation of several kinases and lead to phosphorylation of MAPKs (Zipfel et al., 2004; Rasmussen et al., 2012). Phosphorylated MAPKs in turn phosphorylate and activate downstream transcription factors

Published by the Plant Communications Shanghai Editorial Office in association with Cell Press, an imprint of Elsevier Inc., on behalf of CSPB and CEMPS, CAS.

(TFs) that function in transcriptional regulation of defense responses (Li et al., 2016; Xu et al., 2017; Yoo et al., 2020). However, plant TFs that regulate the expression of *MAPK* genes have not been characterized to date.

More than 30 TFs have been implicated in PTI development in *Arabidopsis thaliana, but* their functional mechanisms have not been fully demonstrated (Thara et al., 1999; Asai et al., 2002; Adachi et al., 2015; Bigeard et al., 2015; Tsuda and Somssich, 2015; Li et al., 2016; Birkenbihl et al., 2018; Huang et al., 2019; Offor et al., 2020). For example, ERF19 and ERF20 were found to be related to resistance induced by the bacterial PAMPs elf18 (Huang et al., 2019) and flg22 (Zhang et al., 2016), respectively, but the related MAPK cascades are not known. Although approximately 30 WRKYs were identified as PAMP-inducible TFs (Birkenbihl et al., 2018), only WRKY29 (Asai et al., 2002) and WRKY33 (Logemann et al., 2013) have been shown to participate in the MPK3/MPK6 cascade to regulate defense responses. To date, only five TFs (ASR3, BES1, ERF6, ERF104, and WRKY33) have been demonstrated to participate in MAPK cascades (Offor et al., 2020). ASR3 functions as a PTI repressor to inhibit the MEKK1–MKK1/2–MPK4 cascade, which, however, promotes immunity activated by MPK4 interactions with resistance proteins containing nucleotide-binding leucine-rich repeats (Li et al., 2015) and inactivation of CCCH zinc-finger proteins (Wang et al., 2022). BES1 (Kang et al., 2015), ERF6 (Meng et al., 2013), ERF104 (Bethke et al., 2009), and WRKY33 (Logemann et al., 2013) support PTI through the MAPKKK3/5–MKK4/5–MPK3/6 cascade (Bi et al., 2018; Liu et al., 2022). In this cascade, BES1, ERF6, ERF104, and WRKY33 function similarly by regulating defense responses following phosphorylation by MPK3 and MPK6 (Bethke et al., 2009; Logemann et al., 2013; Meng et al., 2013; Kang et al., 2015). Evidently, a knowledge gap exists between transcriptional regulation and biochemical function of the cascade, because the TFs that activate *MPK3* and *MPK6* expression to promote kinase production as a prerequisite for the phosphorylation cascade are yet to be determined.

We attempted to fill this gap by searching the literature for *Arabidopsis* TFs that have been implicated in PTI development (Offor et al., 2020) and by determining whether PTI occurs in any of the 37 TF-loss-of-function *Arabidopsis* mutants investigated in our previous studies (Liu et al., 2010, 2011). Out of the 37 TFs, MYB44 was identified as a multifaceted TF involved in growth and defense regulation (Liu et al., 2010, 2011; Nguyen et al., 2012; Shim et al., 2012; Persak and Pitzschke, 2013). MYB44 was shown to interact with MPK3, which phosphorylates it at serine residue S145, and these events are critical for enhancing resistance to osmotic stress (Persak and Pitzschke, 2013). It has been demonstrated that MYB44 is phosphorylated by both MPK3 and MPK6 at S53 and S145, and the MPK3/MPK6-dependent phosphorylation of MYB44 is essential for seed germination (Nguyen et al., 2012). The *MYB44* gene promoter can bind the nuclear import protein VIP1, which activates *MYB44* expression in an MPK3-dependent manner (Pitzschke et al., 2009). MYB44 may be involved in PTI through its function in activating expression of *EIN2* by binding to its promoter (Liu et al., 2011). EIN2 is the central regulator of ethylene signaling not only for plant growth and development but also for innate immunity, including PTI (Boutrot et al., 2010; Mersmann et al., 2010; Tintor et al., 2013; Wang et al., 2018; Zhang et al., 2022). In wild-type (WT) *Arabidopsis* plants treated with a PAMP, *FLS2* gene expression is induced as a critical step for induction of defense responses (Boutrot et al., 2010; Mersmann et al., 2010; Tintor et al., 2013). However, induction of *FLS2* expression and defense responses is seriously compromised in *Arabidopsis ein2 (EIN2-defective) mutants* (Boutrot et al., 2010; Mersmann et al., 2010; Tintor et al., 2013). Here, we show that MYB44 is an integral component of the PTI pathway and confers disease resistance by promoting the expression of *EIN2*, *MPK3*, and *MPK6*.

RESULTS

PAMP-induced resistance is seriously impaired in the *Arabidopsis myb44* mutant

Disease susceptibility and PAMP-induced resistance to the bacterial leaf speck pathogen *Pseudomonas syringae* pv. *tomato* (*Pst*) of 37 TF-defective *Arabidopsis* mutants (Supplemental Figures 1 and 2) characterized in our previous studies (Liu et al., 2010, 2011) were compared with those of the WT. Pure water and an aqueous solution of flg22, a functional fragment of the bacterial PAMP flagellin, were sprayed over the tops of 20-day-old *Arabidopsis* seedlings in the control and induction groups, respectively. After 2 days, plants in both groups were inoculated with a bacterial suspension of the virulent *Pst* strain DC3000 (*Pst* DC3000) by spraying over the tops. Thereafter, the plants were investigated to evaluate disease susceptibility and flg22-induced resistance.

Disease susceptibility was evaluated in the control group using two conventional criteria: (1) bacterial populations of *Pst* DC3000 in leaves 3 days after inoculation (dai), and (2) disease severity at 9 dai quantified as the ratio of necrotic leaf area to total leaf area. On the basis of these criteria, 28 mutants resembled the WT in disease susceptibility, whereas the remaining nine mutants (*myb30*, *myb38*, *myb44*, *myb51*, *myb73*, *myb108*, *k13n2.14*, *hb-7*, and *rap2.6*) were more susceptible than the WT (Supplemental Figures 1 and 2). Differences in disease susceptibility due to the presence or absence of different TFs were clearly revealed by substantial variation in bacterial populations (Supplemental Figure 1A), chlorosis and necrosis symptoms (Supplemental Figure 1B), and disease severity (Supplemental Figure 1C) in leaves of the different plants. Among all the mutants, *myb44* was most susceptible to the pathogen (Supplemental Figures 1A–1C).

Flg22-induced resistance was assessed as the percentage reduction in bacterial populations and disease severity in flg22-treated plants compared with control plants. On the basis of these criteria, 33 mutants exhibited high levels of flg22-induced resistance, similar to the WT plant, but the remaining four mutants (*myb44*, *myb51*, *zfp6*, and *rap2.6*) were compromised in resistance induction (Supplemental Figures 1A–1C and 2). These mutants were also impaired in resistance induction by ch8 (Supplemental Figure 3), a fungal PAMP of the chitin group. Instead, these mutants showed high *Pst* DC3000 bacterial multiplication in leaves and displayed severe symptoms, regardless of whether ch8 was applied before plant inoculation

(Supplemental Figure 3). Among the four mutants, *myb44 showed the most compromised* PAMP-induced resistance (Supplemental Figures 1–3). Clearly, *MYB44*, *MYB51*, *ZFP6*, and *RAP2.6* are required for PAMP-induced resistance against the bacterial pathogen in *Arabidopsis*; however, *MYB44* is the most important. Similar results were obtained from plants inoculated by leaf infiltration, suggesting that reduced PTI in the *myb44* mutant was caused by compromised resistance rather than reduced entry of the bacteria (Supplemental Figure 4). Overall, these results confirm the importance of *MYB44* for disease susceptibility and PAMP-induced resistance.

MYB44 is required for transcriptional regulation of *MPK3* and *MPK6*

According to the accepted model (Bi et al., 2018; Sun et al., 2018; Liu et al., 2022), PTI is regulated by two distinct MAPK cascades: MAPKKK3/5–MKK4/5–MPK3/6 (called the MPK3/6 cascade hereafter) and MEKK1–MKK1/2–MPK4 (Supplemental Figure 5A). We assumed that MYB44 might affect PTI by concomitantly participating in one of the cascades or differentially participating in both. To verify this hypothesis, we determined the expression levels of cascade genes in leaves of WT and *myb44* plants after induction treatment with an aqueous solution of flg22 or ch8 and treatment with water for the control. We found that *MPK4* expression levels showed little change in both WT and *myb44* plants, irrespective of flg22 treatment (Supplemental Figure 5B). By contrast, *MAPKKK3*, *MAPKKK5*, *MEKK1*, *MKK1*, *MKK2*, *MKK4*, and *MKK5* had similar expression levels in control (water-treated) plants, and their expression levels increased greatly in different plants treated with flg22 (Supplemental Figure 5B) or ch8 (Supplemental Figure 5B). Thus, induced expression of these genes does not require MYB44. However, a functional *MYB44* gene was found to be critical for induction of *MPK3* and *MPK6* expression by PAMPs (Figure 1 and Supplemental Figures 5 and 6). The abundance of *MPK3* and *MPK6* transcripts was greater at 10 min after flg22 treatment than at 0 min (immediately) after flg22 treatment in the WT, whereas their abundance showed little change in the *myb44* mutant throughout the experimental period (Supplemental Figure 6A). In the WT, expression levels of *MPK3* and *MPK6* increased maximally by 5.5 and 93 fold, respectively, in the 0–120 min after flg22 application, whereas their expression showed little change in *myb44* during the same period. In the WT, *MPK3* showed the highest expression level at 30 min, and *MPK6* showed a sharp increase in expression at approximately 60 min (Supplemental Figure 6A).

We further analyzed the expression levels of *MPK3* and *MPK6* at 30 and 60 min after induction. At 30 min, flg22 and ch8 treatments increased *MPK3* expression more than 50 and 30 fold, respectively, in all plants except the *myb44* mutant (Figure 1A). Compared with that in the WT, *MPK3* expression in *myb44* was reduced by 40 and 30 fold under flg22 and ch8 treatments, respectively, at 30 min. By contrast, none of the plants showed increased *MPK6* expression under any treatment at 30 min (Figure 1A and Supplemental Figure 5B), and *MPK6* expression did not increase until 60 min (Figure 1A). Up to 60 min, both flg22 and ch8 caused small but significant increases in the expression levels of *MPK6* in WT, *myb51*, *zfp6*, and *rap2.6*; however, *MPK6* expression levels did not increase in *myb44* (Figure 1A). Moreover, both basal and PAMP-enhanced expression of *MPK3* and *MPK6* were impaired (Figure 1A). These analyses suggest that *MYB44* is required for enhancing the PAMP-induced expression of MPK3/6 cascade genes.

To investigate whether PAMP-induced phosphorylation of MPK3 and MPK6 in *myb44* differs from that in other TF-defective mutants (*myb51*, *zfp6*, and *rap2.6*), we analyzed protein extracts from leaves of mutant and WT plants 30 min after treatment with water (control) or an aqueous solution of flg22 or ch8. MAPK phosphorylation was detected by immunoblotting (IB) with a MAPK antibody (α-MAPK) prepared as Phospho-p44/42 MAPK Erk1/2 Thr202/Tyr204 rabbit monoclonal antibody (Figure 1B). In all IB analyses, total leaf proteins were loaded in equivalent amounts, which were verified by staining with Ponceau S (Figure 1B) and IB with the constitutively produced protein, β-tubulin (Figure 1B). Both MPK3 and MPK6 were phosphorylated at low basal levels in all plants treated with water; however, their phosphorylation was considerably increased in WT plants treated with flg22 or ch8 (Figure 1B). However, the degree of MPK3 and MPK6 phosphorylation was markedly reduced in *myb44* compared with that in the WT (Figure 1B and Supplemental Figure 6B). Furthermore, synthesis of MPK3 and MPK6 proteins was found to be substantially impaired in *myb44* relative to that in WT, *myb51*, *zfp6*, and *rap2.6* under the same treatments (Supplemental Figure 6C).

Taken together, these results suggest that activation of *MPK3* and *MPK6* expression by MYB44 and the ensuing production of both MAPK proteins provide the molecular basis for MAPK phosphorylation in response to PAMP.

Genetic complementation of the *myb44* mutant and *MYB44* overexpression in the WT produce stable resistance levels

To verify the role of MYB44 in *Arabidopsis* resistance to *Pst* DC3000, we reassessed the WT and the *myb44* mutant, as well as progenies of previously created *myb44*-complemented (*myb44*/*MYB44*) and *MYB44*-overexpressing (*MYB44*-OE) transgenic *Arabidopsis* lines (Liu et al., 2011). The *myb44*/*MYB44* lines were generated by transformation of the *myb44* mutant with the coding sequence (CDS) of the WT *MYB44* gene fused with its own promoter and the oligonucleotide code of the $His_{(6)}$ tag (Figure 2A). Three *myb44*/*MYB44* lines (#2, #7, and #9), which have been well-characterized previously (Liu et al., 2011), had been propagated to the T7 generation when the present study was initiated. Selfing T7 progenies of the *myb44*/*MYB44*#2, *myb44*/*MYB44*#7, and *myb44*/*MYB44*#9 *Arabidopsis* plant lines were confirmed to stably harbor the backfilled *MYB44-his* gene, which restored *myb44* to WT in terms of *MYB44* expression level (Figure 2B). Indeed, *myb44* complementation was due to the *MYB44-his* fusion gene (Figure 2B), which maintained genetic constancy as shown by stable expression in different *myb44*/*MYB44* lines up to the T7 generation (Supplemental Figure 6A). Complementation also restored the resistance level of *myb44* to that of the WT in terms of *Pst* DC3000 bacterial populations in leaves 3 dai (Figure 2C), necrosis symptoms formed on leaves st 9 dai (Figure 2D), and disease severity scored at 9 dai (Figure 2E and Supplemental Figure 7B).

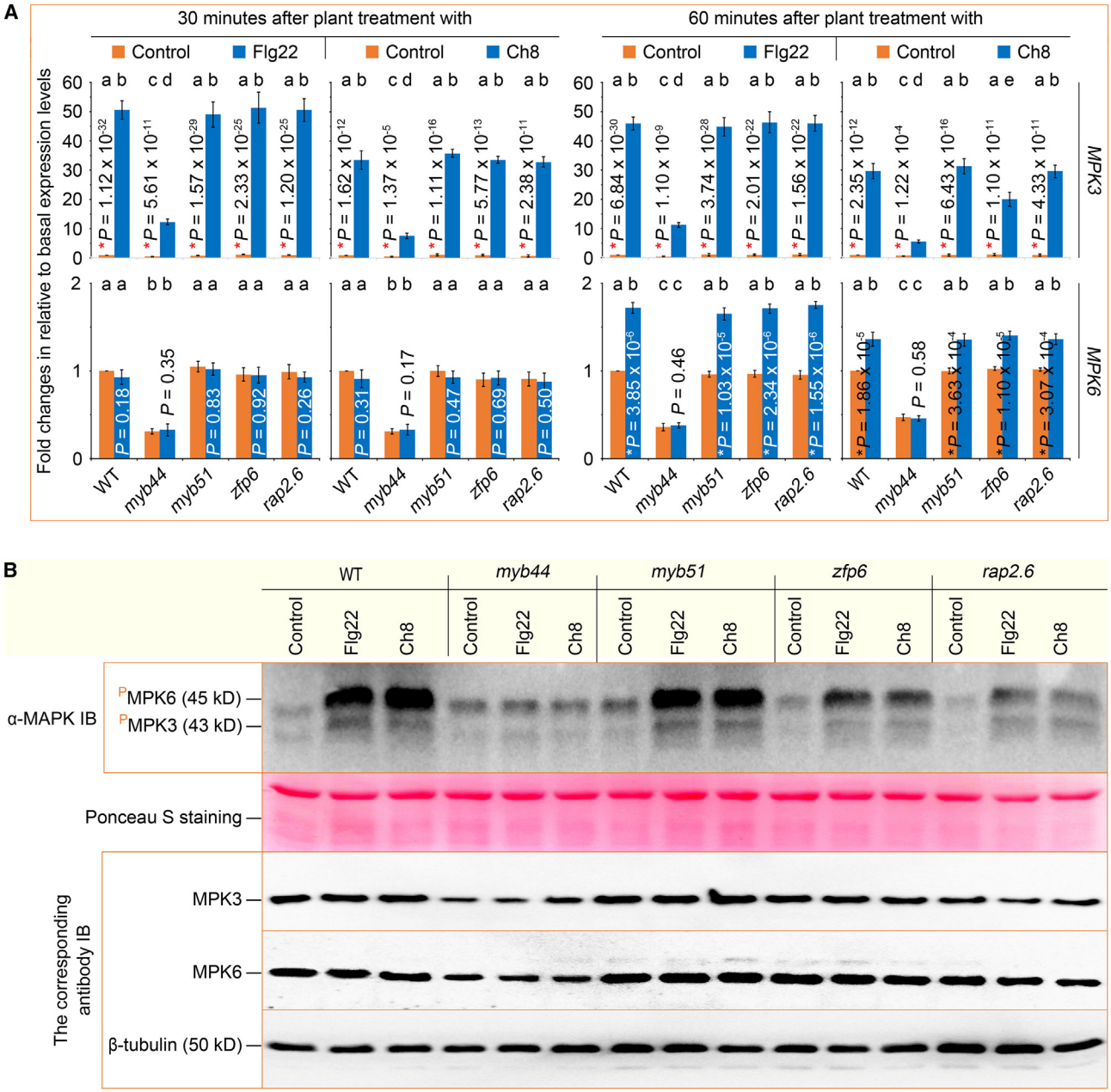

Figure 1. PAMPs fail to efficiently enhance *MPK3* and *MPK6* expression and protein phosphorylation in *myb44*

(A) Changes in *MPK3* and *MPK6* expression levels in leaves of the WT and TF-defective mutant plants after treatment with H_2O (control) or an aqueous solution of flg22 or ch8. Gene expression was analyzed by qRT-PCR, and fold increases in expression level (mean ± SD) were quantified relative to control levels set to 1 in the WT plant. *P* values are based on two-tailed Student's *t*-tests (n = 6, each with five plants), and red asterisks indicate significant differences between the corresponding paired data. In addition to Student's *t*-tests, which were performed to determine whether any of the tested plant genotypes showed different responses to control and PAMP (flg22 or ch8) treatment, analysis of variance and Duncan's new multiple range tests were also performed to assess differences in gene expression levels among the tested genotypes. The results of Duncan's new multiple range tests are presented in the graphs, and different letters indicate significant differences ($P < 0.005$).

(B) Quantitative variation in MPK3 and MPK6 protein production and phosphorylation in leaves of the different plants 30 min after treatments similar to **(A)**. Protein phosphorylation was analyzed by immunoblotting (IB) with α-MAPK. Protein production levels were determined by IB with the indicated antibodies. Uniform loading of total proteins was verified by Ponceau S staining and IB with α-tubulin. Each blot image represents three experimental repeats.

MYB44-OE lines were generated by transformation of WT plants with the *MYB44* CDS fused with a constitutive promoter and the $His_{(6)}$ coding sequence (Figure 2F). Two *MYB44*-OE lines (#1 and #4) have previously shown enhanced resistance against *Pst* DC3000 (Zou et al., 2013). Lines #1 and #4, as well as line #7, which was identified previously (Liu et al., 2011; Zou et al., 2013), had been propagated to the T8 generation when the present study was initiated. We confirmed that *MYB44*-OE#1,

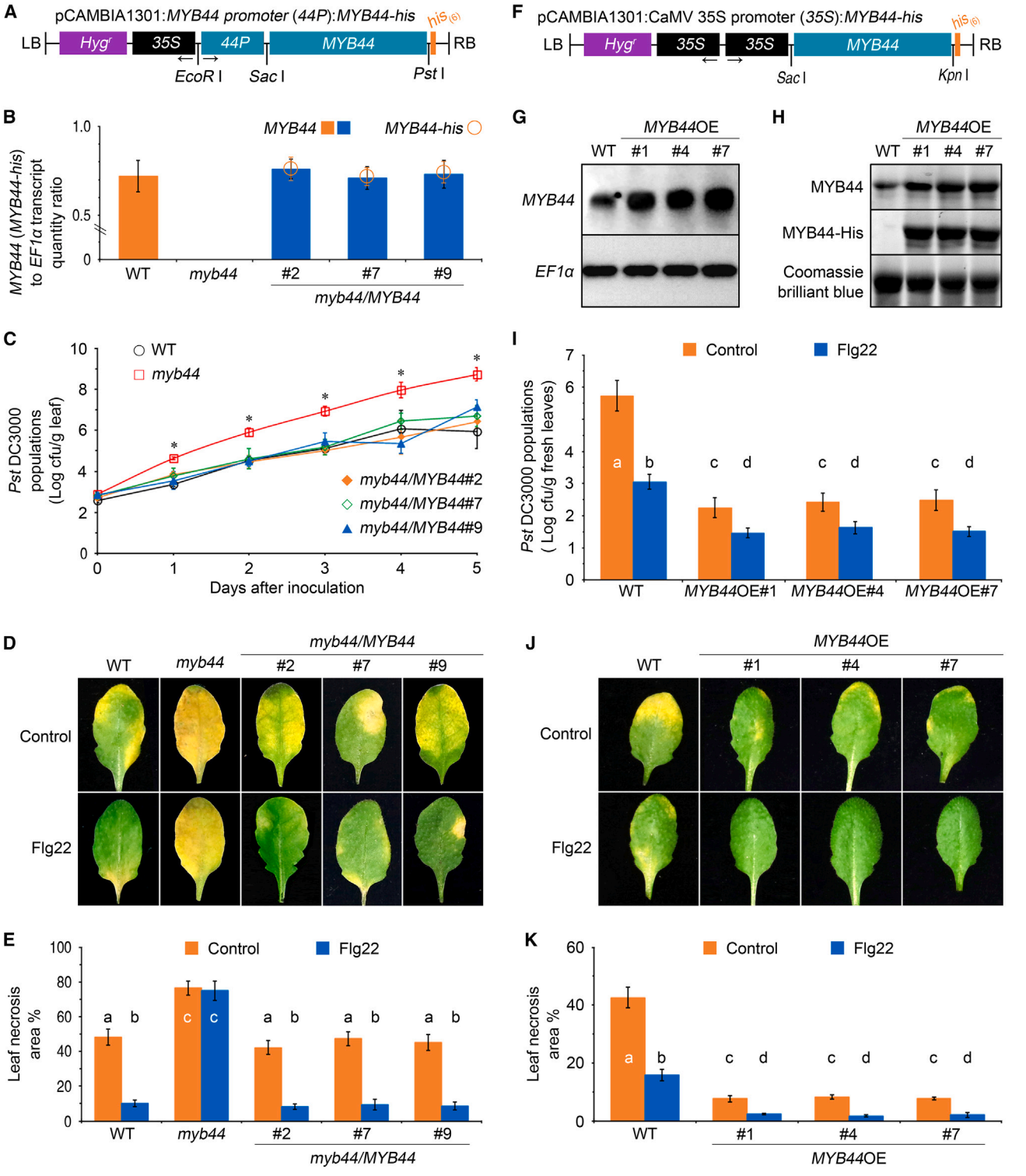

Figure 2. MYB44 contributes to basal and PAMP-induced resistance.

(A) Diagram of the *myb44*-complementation construct.

(B) *MYB44* and *MYB44-his* expression in leaves of different plants. Gene expression was analyzed by qRT-PCR with the constitutively expressed *EF1α* as a reference gene.

(C) Chronological changes in the multiplication of bacterial populations in plant leaves.

(D) Leaf images, each representing 90 leaves 9 days after inoculation (dai) with *Pst* DC3000 and 11 days after treatment with flg22 or the mock reagent (control).

(legend continued on next page)

MYB44-OE#4, and *MYB44*-OE#7 showed more genetic stability upon selfing to the T8 generation compared with that of WT plants (Figure 2G and Supplemental Figure 7A). We further verified that the innate MYB44 protein was produced in greater amounts in *MYB44*-OE lines than in WT plants (Figure 2H). In particular, the MYB44-His fusion protein was produced only in the *MYB44*-OE plants (Figure 2H). Compared with the WT, the *MYB44*-OE lines showed less *Pst* DC3000 bacterial multiplication (Figure 2I). Therefore, leaf necrosis symptoms (Figure 2J) and disease severity (Figure 2K) were considerably reduced in the *MYB44*-OE lines.

Statistical analyses indicated that *Pst* DC3000 bacterial populations and leaf speck disease severity were significantly lower in *myb44*/*MYB44* than in the *myb44* mutant (Figure 2C–2E). Bacterial populations and disease severity were further decreased owing to overproduction of MYB44 protein in the *MYB44*-OE plants, in contrast to those in the WT plant (Figure 2I–2K). In other words, plant resistance was impaired by the *myb44* mutation, rescued by genetic complementation, and enhanced by *MYB44* overexpression (MYB44 overproduction). In essence, the retrieved resistance trait was stably transferred to T7 progenies of the *myb44*/*MYB44 Arabidopsis* lines (Supplemental Figure 7A) at the beginning of this study. Simultaneously, the enhanced resistance trait had been stably transferred to the T8 progenies of the *MYB44*-OE lines (Supplemental Figure 7B). These results confirm the function of MYB44 in conferring basal resistance against the bacterial pathogen in *Arabidopsis*.

MYB44 is required for PTI development

In addition to changes in basal resistance, flg22-induced resistance of the genetically complemented *myb44* transgenic lines was similar to that of the WT. The *myb44*/*MYB44*#2, *myb44*/*MYB44*#7, and *myb44*/*MYB44*#9 lines had sufficient flg22-induced resistance, similar to that of the WT plant, markedly alleviating necrosis symptoms (Figure 2D) and considerably reducing disease severity (Figure 2E) in the complemented plants compared with the *myb44* mutant. By contrast, the *myb44* mutant was highly susceptible to the disease and showed severe symptoms (Figure 2D and 2E), regardless of whether flg22 was applied. Clearly, *MYB44* is essential for flg22-induced resistance against the bacterial pathogen in *Arabidopsis*. Compared with that in the WT, flg22-induced resistance in the *MYB44-OE#1, MYB44-OE#4, and MYB44-OE#7 transgenic lines* was further enhanced by *MYB44* overexpression. Resistance induced by flg22 was greater in these *MYB44*-OE lines than in the WT, repressing bacterial multiplication (Figure 2I), alleviating necrosis symptoms (Figure 2J), and decreasing disease severity (Figure 2K). These results confirmed that a functional *MYB44* is required for induction of resistance by flg22.

A functional *MYB44* is also required induction of reactive oxygen species (ROS) production by flg22, and ROS promote PTI development in response to PAMPs (Tian et al., 2016; Zhang et al., 2022). In *Arabidopsis* plants sprayed with an aqueous flg22 solution containing the surfactant Silwet L-77, ROS were initially produced in single leaves at 5 min, accumulated in more leaves from 10–35 min, and were produced in the entire plant in the subsequent 10 min (Figure 3A). WT and *myb44*/*MYB44* plants performed moderately; *myb44* was nullified, but *MYB44*-OE exceeded both WT and *myb44*/*MYB44* in the rate and quantity of ROS production and accumulation (Figure 3A). In 45 min, ROS (Figure 3B), particularly H_2O_2 (Figure 3B inset), accumulated to the highest levels in *MYB44*-OE plants compared with WT and *myb44* plants. Spraying plants with pure water, with or without Silwet L-77, also induced ROS; however, the rate of ROS production and amount of ROS accumulation were lower than those in plants sprayed with flg22 (Supplemental Figure 8).

MYB44 was also found to be critical for flg22 induction of defense responses characteristic of the MPK3/6 cascade (Figure 3C–3E and Supplemental Figures 6 and 9). The ability of PAMPs to induce expression of *MPK3* and *MPK6* was inhibited in the *myb44* mutant, but *myb44*/*MYB44* and WT plants showed similar flg22-induced expression of both *MAPKs* (Supplemental Figure 6A). Among all genotypes, the *MYB44-OE plants showed the strongest* induction of *MPK3* and *MPK6* expression by flg22 (Supplemental Figure 6A). In response to flg22, defense response genes that are regarded as molecular markers of earlier (Figure 3C) and later (Supplemental Figure 9) PTI development were highly expressed in *myb44*/*MYB44* plants, similar to the WT, and their expression levels were further increased in *MYB44*-OE plants. Expression levels of marker genes for earlier stages of PTI development—*FRK1*, *NHL10*, *PHI-1*, and *WRKY53* (Sardar et al., 2017)—were increased 10–100 fold in the WT and *myb44*/*MYB44* plants and increased by additional 10 fold in *MYB44*-OE lines at 2 h after flg22 application (Figure 3C). Expression of marker genes for later stages of PTI development—*PAL1*, *PAL2*, *GSL5*, and *GSL6* (Wu et al., 2019; Chen et al., 2021)—was increased 5–55 fold in WT or *myb44*/*MYB44* plants and further increased in *MYB44*-OE plants at 6 h (Supplemental Figure 9). Thus, flg22 acted in a MYB44-dependent manner to induce the expression of different PTI marker genes. In particular, *GSL5* and *GSL6* have been shown to be essential for callose production (Lü et al., 2011), and callose deposition is a universal response that is also involved in PTI (Clay et al., 2009; Luna et al., 2011; Xu et al., 2016). We found greater callose deposition in *MYB44*-OE plants than in WT and *myb44*/*MYB44* plants (Figure 3D), which occupied a larger area (Figure 3D) with a greater amount (Figure 3E) on the surface of *MYB44*-OE leaves. By contrast,

(E) Quantification of disease severity at 9 dai.
(F) Diagram of the *MYB44*-overexpression construct.
(G) Northern blotting of leaf RNA hybridized with a *MYB44* probe and a probe specific to the *EF1α* gene used as a reference.
(H) IB of leaf proteins showing the presence of MYB44 and MYB44-His, and blot staining to verify uniform loading. MYB44-His was detected by hybridization with a commercial anti-His antibody. MYB44 was detected by hybridization with a specific anti-MYB44 antibody produced by immunizing rabbit.
(I–K) Evaluation of *Pst* DC3000 virulence based on bacterial populations in leaves 3 dai **(I)** and on leaf symptoms **(J)** and disease severity **(K)** at 9 dai. **(C, I, E, and K)** Data shown are means ± SDs (n = 6, each with 15 leaves from five plants); data were analyzed using Duncan's new multiple range test ($P < 0.005$). Asterisks indicate significant differences between *myb44* and the other plants **(C)**. Different letters indicate significant differences among the different plants **(I, E, and K)**.

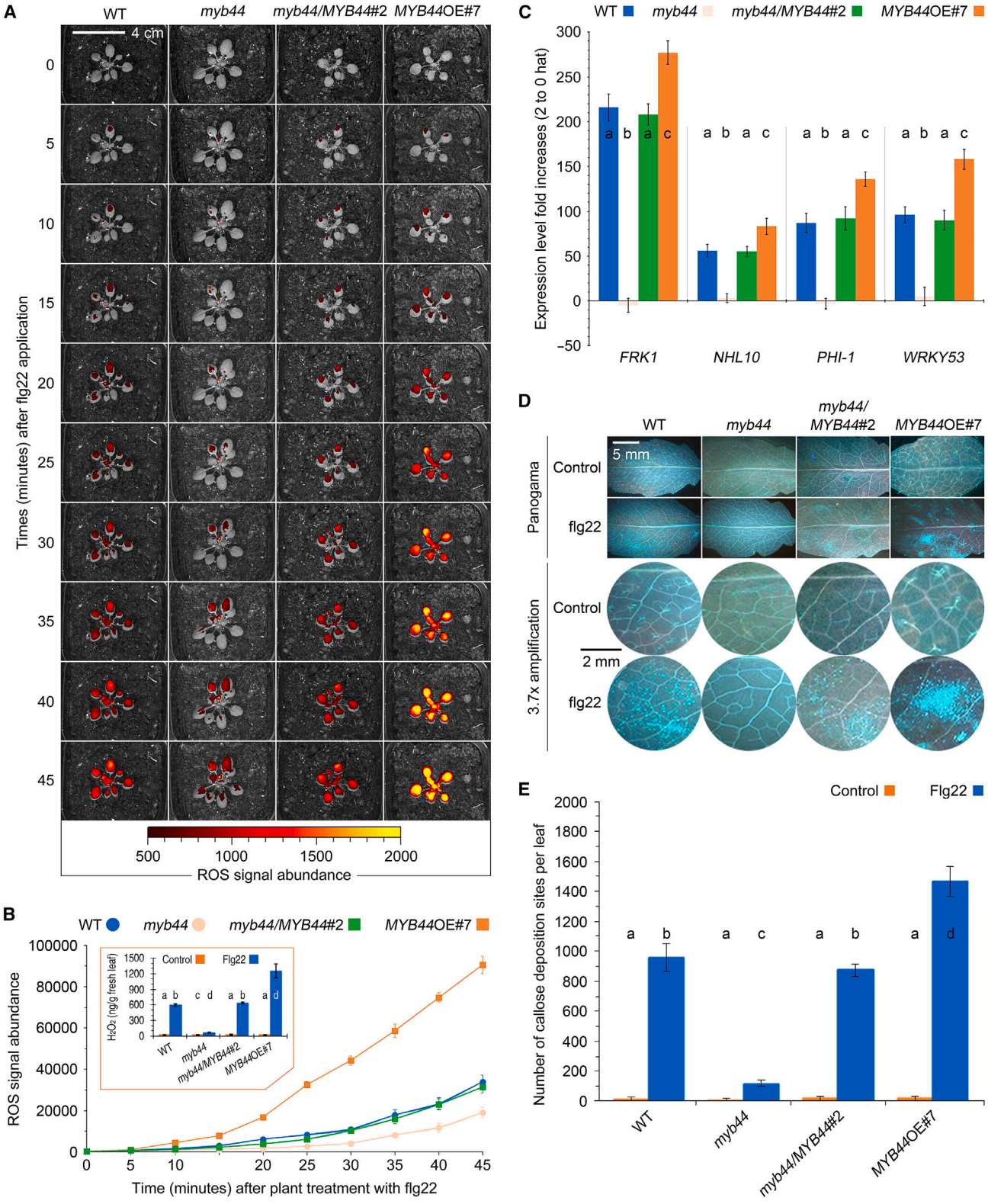

Figure 3. *MYB44* is required for PTI development.

(A) Visualization of reactive oxygen species (ROS) in plants of *MYB44*-related genotypes by staining with 2,7-dichlorofluorescein diacetate (DCF) at the indicated times after treatment with flg22. Each plant image represents 15 plants from three experimental repeats.

(B) Chronological changes in relative levels of ROS quantified as DCF-staining signal densities in plants as in **(A)**. Inset shows H_2O_2 concentrations in plants 45 min after treatment. Data are means ± SDs (n = 3, each with five plants).

(legend continued on next page)

flg22 failed to induce defense-responsive gene expression and callose deposition in the *myb44 mutant* (Figure 3C–3E). Thus, MYB44 is required for PTI development, as shown by ROS production and induction of defense responses.

MYB44 affects MPK3 and MPK6 phosphorylation by activating both *MAPK* genes

To determine the functional relationship between MYB44 and MPK3/6 in the PTI pathway, we analyzed related *Arabidopsis* genotypes, including the *GVG:DD* transgenic line, in which MPK3 and MPK6 phosphorylation is enhanced under dexamethasone (DEX) treatment (Wang et al., 2007). The conditional *mpk3 mpk6* (*mpk3/6*) double mutant (Ren et al., 2008; Xu et al., 2014) was also tested. At the transcriptional level, *MYB44* expression was enhanced by flg22 to a similar extent in the WT, the *mpk3* and *mpk6* single mutants, and the conditional *mpk3/6* double mutant (Figure 4A). *GVG:DD* plants did not show evident changes in flg22-induced *MYB44* expression (Figure 4A). Therefore, single or concurrent disruption or activation of *MPK3* and *MPK6* did not affect the ability of flg22 to induce *MYB44* expression. By contrast, *MPK3* and *MPK6* expression was considerably enhanced by flg22 in a *MYB44*-dependent manner (Figure 4B). Their expression was greatly enhanced in *MYB44*-OE plants but considerably impaired in the *myb44* mutant compared with the moderate expression found in WT and *myb44/MYB44* plants (Figure 4B). MAPK protein production and phosphorylation levels showed similar patterns (Figure 4C). Phosphorylation of MPK3 and MPK6 was induced by flg22 in WT, *myb44/MYB44*, and *MYB44*-OE plants but not in the *myb44* mutant, in which MPK3 and MPK6 proteins were produced in small amounts (Figure 4C). Compared with the WT and *myb44/MYB44* plants, *MYB44*-OE showed greater induction of MPK3 and MPK6 phosphorylation by flg22 (Figure 4D). Thus, MYB44 functions upstream of MPK3/6 in the PTI pathway. Moreover, flg22 induced the phosphorylation of MPK3 and MPK6 proteins while affecting the expression of both the *MAPK* genes, which displayed *MYB44*-dependent increases in expression after PAMP application in WT, *myb44/MYB44*, and *MYB44*-OE plants (Supplemental Figure 6A). In these plants, expression of *MPK3* and *MPK6* genes (Supplemental Figure 6A) and phosphorylation of both MAPK proteins (Figure 4C) occurred quickly (in 10 min) after PAMP application. Furthermore, flg22 induced MPK4 phosphorylation in a MYB44-dependent manner, although phosphorylation intensity was considerably lower in MPK4 than in MPK3 and MPK6 (Figure 4C).

The promoters of *MPK3* and *MPK6* contain the previously identified consensus MYB recognition motif AAACCA (Serpa et al., 2007), suggesting that MYB44 may activate the expression of *MPK3* and *MPK6* by directly targeting their promoters. This speculation was verified by chromatin immunoprecipitation (ChIP) assays with pertinent *Arabidopsis* genotypes. The *myb44* mutant was complemented with the CDS of the WT *MYB44* gene fused to its own promoter and $his_{(6)}$ (Liu et al., 2011). The *myb44*-complemented lines were confirmed to produce large amounts of MYB44-His fusion protein (Figure 2H). In response to flg22 or ch8, MYB44-His bound directly to the promoters of *MPK3* (Supplemental Figure 10A) and *MPK6* (Figure 4E and 4F), activating their expression (Figure 4G). Both ChIP PCR (Figure 4E and Supplemental Figure 10B) and ChIP qPCR (Figure 4F) demonstrated that MYB44-His bound to the *MAPK* promoter. By contrast, MYB44-His did not bind to the CDS of *MPK3* or *MPK6* (Supplemental Figure 10B).

Expression of *MPK3* and *MPK6* was also activated by $MYB44^{DD}$, the constitutively active form of MYB44 generated by replacing 53S and 145S with L-aspartic acid (Nguyen et al., 2012). $MYB44^{DD}$ could bind to the promoters of *MPK3* and *MPK6* (Figures 4E and 5F, Supplemental Figure 10A) and activate the expression of both *MAPK*s (Figure 4G) in *myb44/*$MYB44^{DD}$*-his* plants with and without PAMP treatment. *MPK3* and *MPK6* were constitutively expressed in *myb44/*$MYB44^{DD\text{-}his\ plants}$, and their relative expression levels were significantly higher after treatment with flg22 or ch8 (Figure 4G). By contrast, both PAMPs failed to enhance the expression of *MPK3* and *MPK6* in *myb44* plants transformed with $MYB44^{AA}$*-his* (Figure 4F), in which $MYB44^{AA}$ was generated by substituting 53S and 145S in the original MYB44 sequence with the phosphodeficient residue arginine (Nguyen et al., 2012). $MYB44^{AA}$-His did not bind to the MAPK promoters (Figure 4E and Supplemental Figure 10A). In this case, flg22 and ch8 did not enhance the expression of *MPK3* and *MPK6* (Figure 4F). These analyses suggest that MYB44 activates the expression of both *MAPK* genes by directly binding to their promoters and that MYB44 executes this function only in the phosphorylated form.

MYB44 is phosphorylated by MPK3 and MPK6 to support PTI

We wanted to know whether MPK3 and MPK6 directly phosphorylate MYB44 to activate its function in providing immunity. In *in vivo* luciferin (Luc) imaging assays, the Luc^{N}-MPK3 fusion protein generated by linking the Luc N-terminal half to MPK3 had a strong interaction with the Luc^{C}-MYB44 protein generated by fusing the Luc C-terminal half to MYB44 (Figure 5A). An interaction also occurred between Luc^{N}-MPK6 and Luc^{C}-MYB44 (Figure 5A). Both protein–protein interactions were specific, and no interaction occurred between protein combinations in the controls (Figure 5A), thus providing the molecular basis for phosphorylation of MYB44 by MPK3 and/or MPK6 in response to PAMP treatment.

The Phos-tag assay is an efficient method for detecting protein phosphorylation on the basis of reduced electrophoretic mobilities of phosphorylated proteins compared with their non-phosphorylated counterparts (Nagy et al., 2018). To determine whether flg22 induces MYB44 phosphorylation and whether

(C) Changes in transcript levels of defense response genes known as early PTI markers in leaves of flg22-treated plants 2 h after treatment (hat) compared with those at 0 hat (immediately after treatment). Data are shown as means ± SDs ($n = 6$, each with 15 plants); different letters indicate significant differences among different plants based on Duncan's new multiple range test ($P < 0.001$).

(D and E) Callose deposition on leaf surfaces at 24 hat. In **(D)**, leaf images are shown on top two rows, and the lower two row include close-up images created by amplifying the lower left 1/4 leaf area of 1 mm^2. In **(E)**, different letters on the graph indicate significant differences based on Duncan's new multiple range test ($P < 0.001$; $n = 6$, each with 300–350 cells).

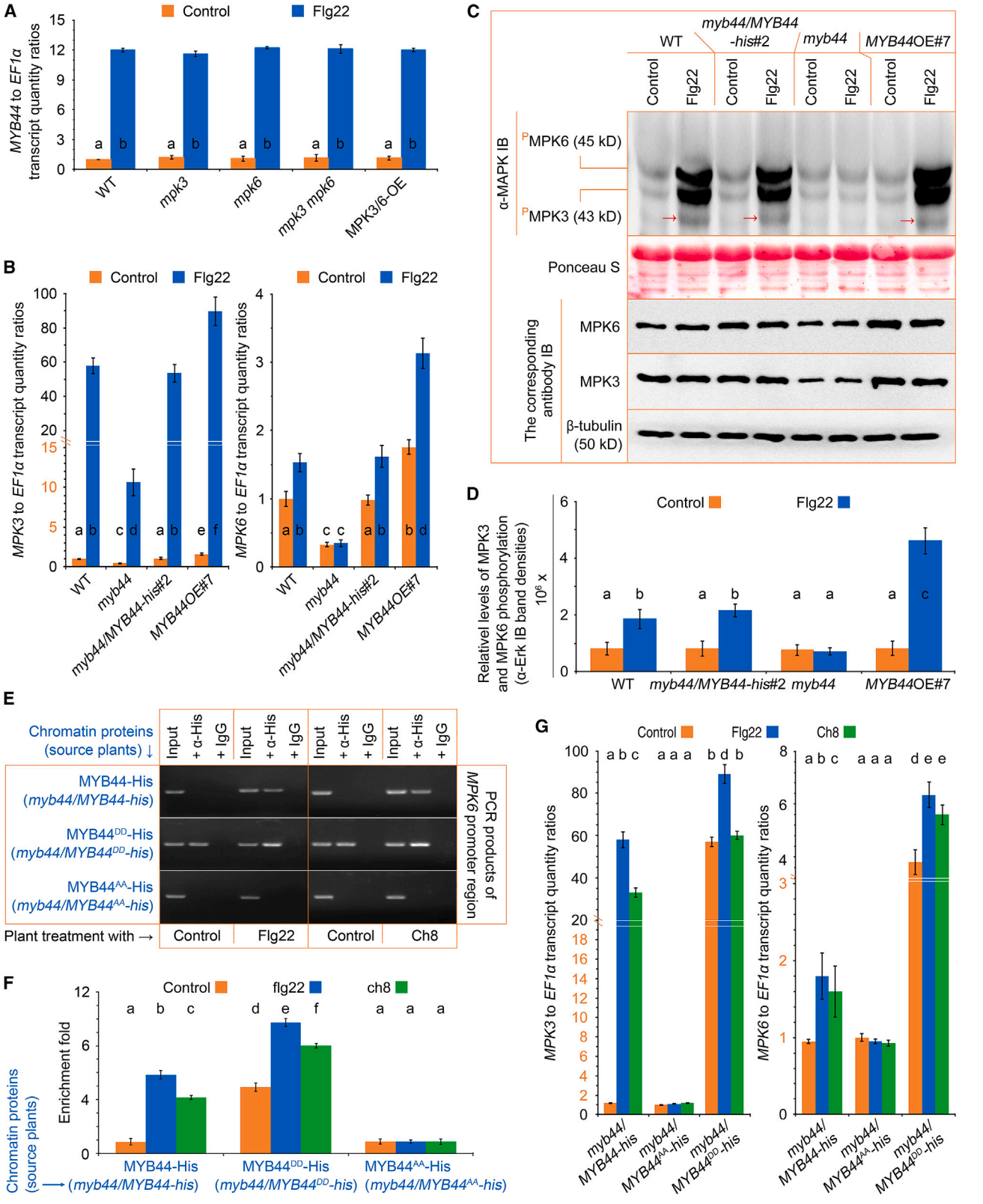

Figure 4. MYB44 activates *MPK3/6* expression to promote kinase phosphorylation.

(A–G) *MYB44*-related plants were treated with water (control), an aqueous solution of flg22 (Flg22), or an aqueous solution of ch8 (Ch8) and then used in the following assays. **(A and B)** *MYB44* and *MAPK* expression in *MYB44*-related plants 30 **(A)** or 60 **(B)** minutes after treatment. Gene expression was analyzed by qRT-PCR with *EF1α* as the reference gene. **(C and D)** Presence or absence of MPK3 and MPK6 phosphorylation in *MYB44*-related plants

(legend continued on next page)

MPK3 and MPK6 are required, we performed Phos-tag assays on WT, *mpk3*, *mpk6*, and *mpk3/6* plants transformed with the *MYB44-his* fusion gene and treated with flg22. On the basis of Phos-tag α-His IB of proteins extracted from leaves and tested at equal amounts, flg22 treatment effectively induced phosphorylation of the MYB44-His fusion protein in the presence of functional *MPK3* or *MPK6* (Figure 5B). MYB44-His was phosphorylated in WT plants at 5 and 30 min after treatment (mat) with flg22; however, no phosphorylation signals were detected at 0 mat (immediately before flg22 treatment). MYB44-His phosphorylation was also induced by flg22 in the *mpk3* and *mpk6* single mutants but not in the *mpk3/6* double mutant (Figure 5B). Thus, MPK3 and MPK6 are required for induction of MYB44 phosphorylation by flg22.

We next determined whether phosphorylation of MPK3 and MPK6 was necessary for their phosphorylation of MYB44. It has been shown that MPK3 and MPK6 can be activated by the expression of $MKK5^{DD}$, a constitutively active form of MKK5 created by replacing threonine 215 and tyrosine 221 with aspartic acid (Li et al., 2017). Using a prokaryotic expression system, $MKK5^{DD}$ was expressed together with MPK3 or MPK6 linked to a haemagglutinin (HA) tag and with MYB44-His or $MYB44^{AA}$-His (Figure 5C). On the basis of Phos-tag α-His IB, MYB44-His was phosphorylated only when $MKK5^{DD}$ was present in combination with phosphorylated MPK3-HA or MPK6-HA; however, $MYB44^{AA}$-His did not exhibit phosphorylation in any protein combination (Figure 5C). In essence, these results suggest that MPK3 and MPK6 must be phosphorylated in order to phosphorylate MYB44.

Next, we assessed the abilities of MPK3-HA and MPK6-HA to phosphorylate MYB44-His *in vivo* in *myb44/MYB44-his#2* (Figure 2D) plants transformed with the *HA* gene (control) or the fusion genes *MPK3:HA* and *MPK6:HA*. MYB44 did not display evident phosphorylation in plants transformed with *HA* or in those transformed with *MPK3:HA* or *MPK6:HA* but not treated with flg22 (Figure 5D). After flg22 treatment, high levels of MPK3 and MPK6 phosphorylation were detected by α-MAPK IB of protein extracts from *myb44/MYB44*#2 seedlings transformed with *MPK-HA* or *MPK6-HA* (Figure 5D). Phos-tag α-His IB of the same proteins revealed that MYB44 was effectively phosphorylated by MPK3-HA and MPK6-HA (Figure 5D). However, MYB44 phosphorylation was nearly eliminated when calf intestinal alkaline phosphatase was applied to the protein extracts (Figure 5D). Phosphatase application also led to inhibition of MPK3 and MPK6 phosphorylation (Figure 5D). These analyses suggest that MPK3 and MPK6 phosphorylate MYB44 in response to flg22 treatment.

We next analyzed expression of defense response genes in leaves of *myb44/MYB44-his#2* plants expressing *HA*, *MPK3:HA*, or *MPK6:HA* and treated with pure water (control) or an aqueous solution of flg22. Expression levels of marker genes for earlier stages of PTI (*FRK11*, *NHL10*, *PHI-1*, and *WRKY53*) and later stages of PTI (*PAL1*, *PAL2*, *GSL5*, and *GSL6*) were greatly enhanced by flg22 treatment compared with the control in all plants, and the degree of enhancement was higher with *MPK3:HA* or *MPK6:HA* compared with *HA*, which was used as an inactive gene reference (Supplemental Figure 11). These results demonstrate that genetic cooperation of *MYB44* with both *MPK3* and *MPK6* is critical for complete activation of the PTI pathway.

MYB44-dependent PTI involves *EIN2* and *FLS2*

In response to flg22, *MYB44* was related to the expression of *EIN2* and *FLS2* genes. Both *EIN2* and *FLS2* were strongly expressed in the concurrent presence of functional *MYB44* (in the WT or in *myb44/MYB44-his*) and flg22 treatment, and flg22-enhanced *EIN2* and *FLS2* expression was further enhanced by *MYB44* overexpression (Figure 6A). By contrast, there was little accumulation of *EIN2* and *FLS2* transcripts in control (water-treated) plants or the *myb44* mutant (Figure 6A). MYB44-dependent flg22-induced expression of *EIN2* and *FLS2* showed quantitative chronological changes (Figure 6B) that were highly consistent with the expression patterns of *MPK3* and *MPK6* after flg22 application (Supplemental Figure 6A). Thus, *EIN2* and *FLS2* displayed different chronological changes in expression pattern in WT, *myb44/MYB44-his*, and *MYB44*-OE plants (Figure 6B). In these plants, expression levels of *EIN2* increased for 2 h after flg22 application (Figure 6, body), whereas those of FLS2 peaked in 15 min and then declined (Figure 6, inset), consistent with the function of *FLS2* at early stage of PTI signal transduction (Zipfel, et al., 2004).

It has been shown that *EIN2* is required for PAMP-induced expression of *FLS2* (Tintor et al., 2013) and, consequently, for expression of defense-related genes (Liu et al., 2011). Consistent with these findings, we found that *EIN2* was critical for flg22 induction of *FLS2* and PTI response genes—*FRK1*, *NHL10*, *PHI-1*, and *WRKY53* (Figure 6C)—which are molecular makers of PTI (Sardar et al., 2017). We also found that the *EIN2* loss-of-function mutation, *ein2-5* (Alonso et al., 1999), inhibited flg22-induced phosphorylation of both MPK3 and MPK6 (Figure 6D). Both MAPKs were strongly phosphorylated in WT plants, whereas MAPK phosphorylation decreased in the *ein2-5* mutant 30 min after flg22 treatment (Figure 6D; Supplemental Table 1). Interestingly, MPK3 and MPK6 were substantially phosphorylated 10 min after flg22 application in the mutant, but

10 min after treatment with flg22 or water (control). Phosphorylation was analyzed at the time when *MPK3* and *MPK6* expression was substantially induced by flg22 (Supplemental Figure 6A). In **(C)**, phosphorylated MPK3 and MPK6 are shown as ^{P}MPK3 and ^{P}MPK6, and arrowheads indicate MPK4 phosphorylation at low levels. The production of MPK3 and MPK6 was determined by IB with the corresponding antibodies. Uniform loading was verified by Ponceau S staining and hybridization with β-tubulin antibody. In **(D)**, phosphorylation levels of MPK3 and MPK6 are quantified as sum values in the different plants shown under the graph. **(E)** ChIP PCR analyses were used to verify that MYB44 binds to the promoters of *MPK3* and *MPK6*. Chromatin was isolated from leaves of different plants 60 min after treatment. Input, DNA fragments from chromatin extracts before immunoprecipitation; +α-His, DNA fragments from chromatin extracts precipitated using the specific antibody α-His; +IgG, DNA fragments from chromatin extracts that underwent precipitation in the presence of the non-immune IgG protein, but not α-His. **(F)** Chromatin samples from **(E)** were used in ChIP qPCR analyses that were performed to confirm MYB44 binding to the *MPK6* promoter. **(G)** qRT-PCR analyses were performed using RNA extracts from plants treated as in **(E)** to verify that MYB44 promotes *MAPK* expression. **(A, B, D, F, and G)** Different letters on bar graphs indicate significant differences based on Duncan's new multiple range test at $P < 0.005$ ($n = 3$, each with 15 plants).

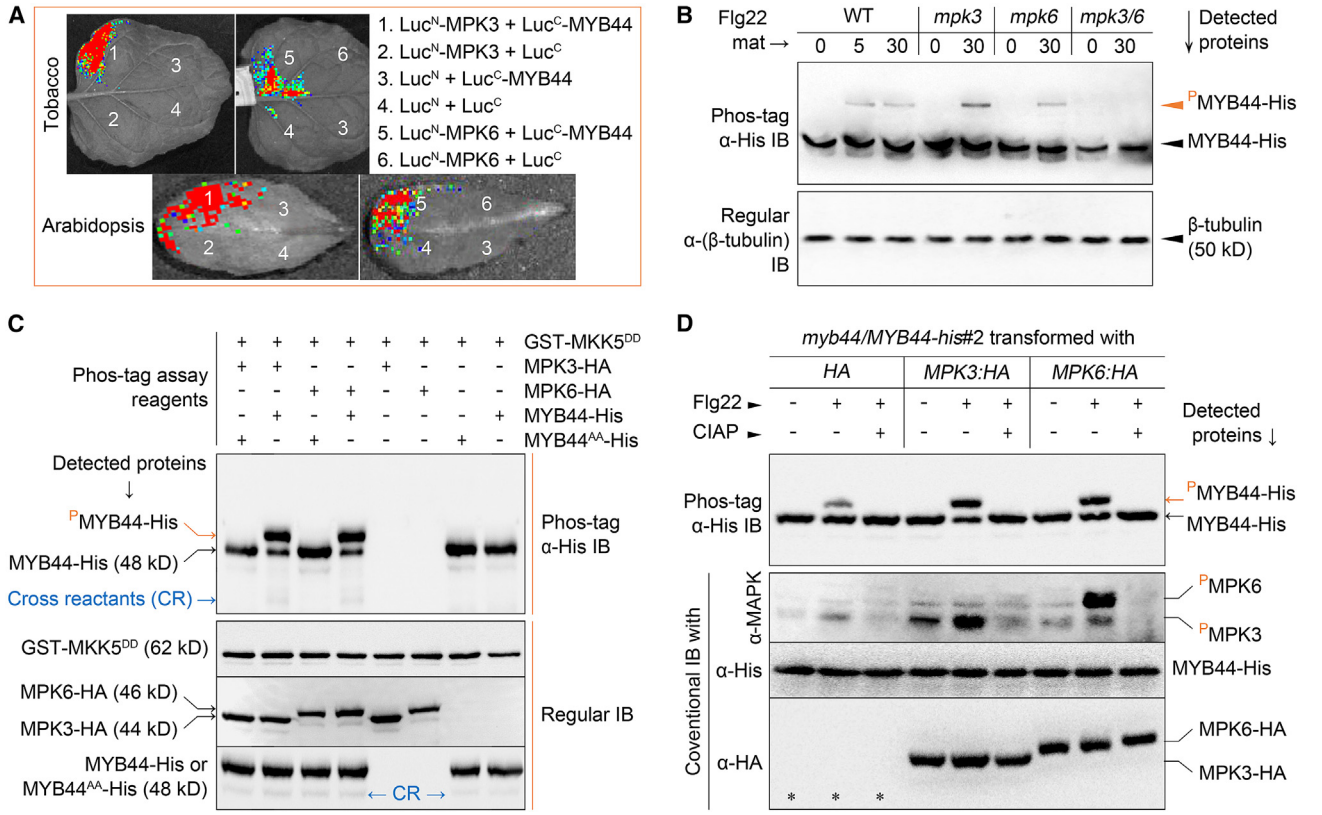

Figure 5. MYB44 is phosphorylated by MPK3 and MPK6.

(A) *In vivo*luciferin image assays of MYB44, MPK3, MPK6, and control proteins in tobacco and *Arabidopsis* leaves. Color changes from blue to red represent increasing intensity of the interaction signal.

(B) Phosphorylation of MYB44 by MPK3 and MPK6. Proteins were isolated from flg22-treated WT and mutant plants, analyzed using Phos-tag to show the phosphorylated and nonphosphorylated proteins, and analyzed by IB to verify uniform loading.

(C) Phos-tag and IB assays of MYB44 and MYB44^{AA} in combination with MPK3 or MPK6 that had been activated via phosphorylation by GST-MKK5^{DD}. All proteins were produced in a prokaryotic expression system and were analyzed in combinations. MYB44 was detected using Phos-tag α-His IB (top blot) to show phosphorylation or by conventional α-His IB (bottom blot) to confirm uniform loading. GST-MKK5^{DD} and MAPK-HA (MPK3-HA and MPK6-HA) were detected using IB with α-GST (middle upper) and α-HA (bottom lower) antibodies, respectively.

(D) Phos-tag and conventional IB assays of MYB44-His and MAPK-HA (MPK3-HA and MPK6-HA) from different transformed plants. Proteins were isolated from plants with or without prior flg22 treatment and incubated with or without phosphatase (an inhibitor of protein phosphorylation). MYB44 phosphorylation was detected by Phos-tag α-His IB (top blot). IB with α-MAPK was used to assess MPK3 and MPK6 phosphorylation. IB with α-His (middle) and α-HA (bottom) was used to indicate the presence or absence of the corresponding proteins, and asterisks indicate that HA was too small (1.1 kDa) to detect.

flg22-induced phosphorylation of MPK3 and MPK6 was abolished after 20 and 30 min, respectively (Figure 6E). By contrast, MPK3 and MPK6 phosphorylation displayed a chronologically stable pattern in the WT for 30 min after flg22 application, and phosphorylation levels declined only at 60 min (Figure 6E). After 60 min, defense response genes could be expressed as a downstream event of PTI signal transduction (Figure 4C and Supplemental Figure 9). These analyses suggest that EIN2 participates in the MYB44-dependent development of PTI at the stage of MPK3/6 phosphorylation.

DISCUSSION

Plant innate immunity systems comprising different signaling pathways are deployed under sophisticated regulation, including intricate interplays among distinct pathways (Li et al., 2021; Ngou et al., 2021; Yuan et al., 2021) and multiple regulatory mechanisms applied to a particular pathway (Zhang and Zhou, 2010; Zhang et al., 2020). Transcriptional regulation provides a core scaffold at the midstream of the PTI pathway to control signaling and intensity of the defense response (Tsuda and Somssich, 2015; Li et al., 2016). According to previous studies on TFs implicated in PTI and the multifaceted roles of MYB44 in plant defense against pathogens, MYB44 was screened out of 37 TF-defective *Arabidopsis* mutants based on its positive effects on basal resistance and PTI responses (Figures 1, 2, 3, and Supplemental Figures 1–7). Further studies disclosed the functional relationships between MYB44 and the MPK3/6 cascade (Figures 4, 5, and Supplemental Figures 8–11) and between MYB44 and EIN2, which is the central regulator of ethylene signaling required for PAMP recognition and PTI development (Boutrot et al., 2010; Mersmann et al., 2010; Liu et al., 2011; Tintor et al., 2013; Ye et al., 2015; Zhang et al., 2021).

On the basis of these analyses, we propose a model in which MYB44 cooperates with the MPK3/6 cascade and EIN2

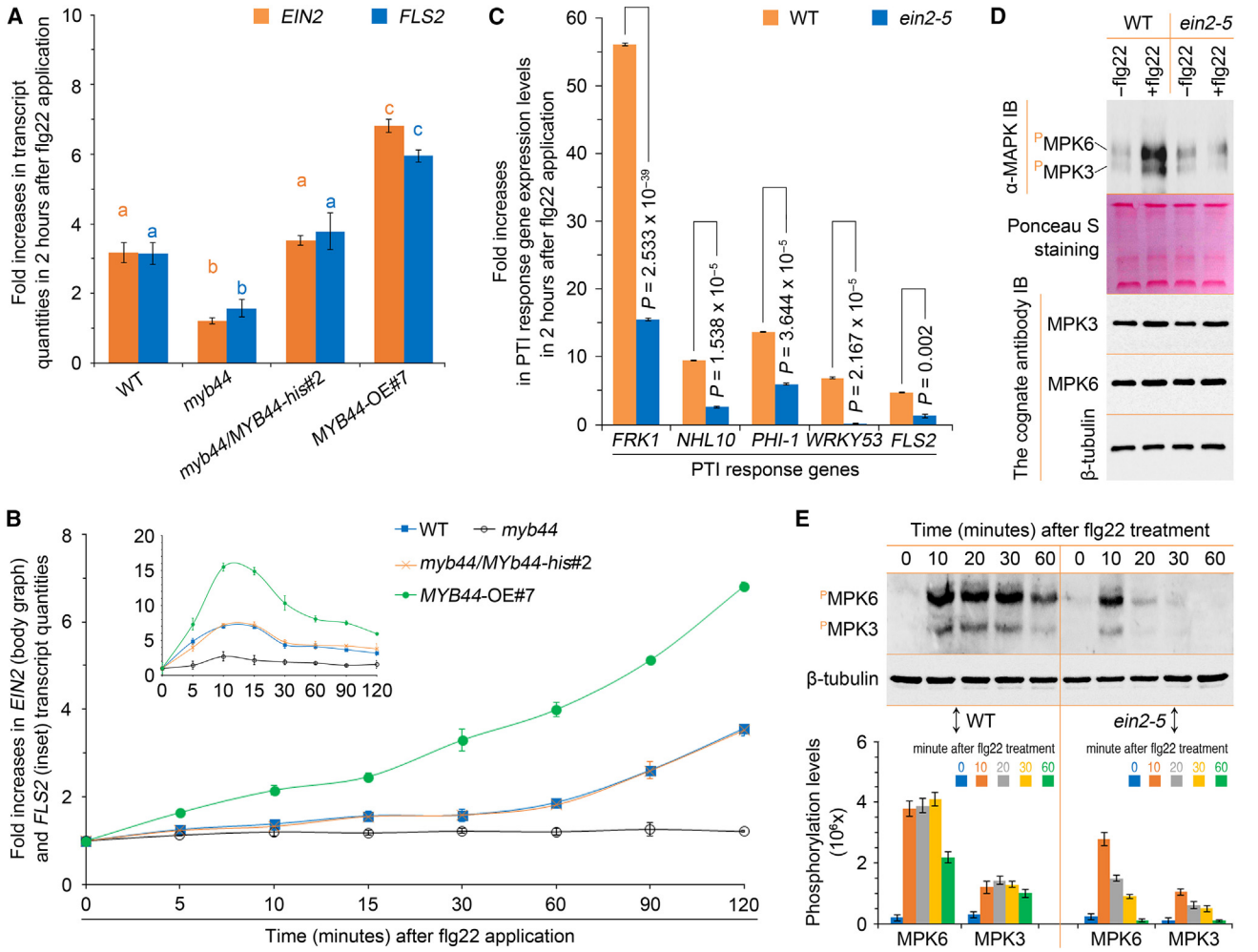

Figure 6. *MYB44* and *EIN2* are related to flg22-induced expression of *FLS2* and PTI-related defense genes and phosphorylation of MPK3 and MPK6.

(A–C) Fold increases in gene expression levels at different time points after treatment with an aqueous solution of flg22. Data are shown as mean values ± SDs (n = 3, each with 15 plants). In **(A)**, different letters in orange and blue indicate significant differences based on Duncan's new multiple range tests (P < 0.001) comparing expression levels of *EIN2* and *FLS2*, respectively. In **(B)**, *EIN2* expression is provided as the main curve graph, while *FLS2* expression is shown in inset. In **(C)**, P values are based on two-tailed Student's t-tests.

(D) Protein production and phosphorylation of MPK3 and MPK6 in leaves of different plants 30 min after treatments similar to those in **(A)**. Protein phosphorylation was analyzed by IB with α-MAPK, a specific antibody against phosphorylated MAPKs prepared as Phospho-p44/42 MAPK Erk1/2 Thr202/Tyr204 D13.14.4E XP Rabbit mAb (Cell Signaling Technology). Protein production levels were determined by IB with the indicated antibodies. Uniform loading of total proteins was verified by Ponceau S staining and IB with α-tubulin. Each blot image represents three experimental repeats.

(E) Chronological changes in the phosphorylation levels of MPK3 and MPK6 after plant treatment similar to that in **(A)**. Uniform loading of total proteins was verified by IB with α-tubulin. Relative levels of MPK3 and MPK6 phosphorylation are shown as means ± SDs of phosphorylation signal density quantified with an imaging system scanner (n = 3, each with 10 plants).

to regulate PTI development in *Arabidopsis* (Figure 7). Upon application, PAMPs simultaneously induce expression of *MYB44*, *MPK3*, and *MPK6*, leading to protein production in *Arabidopsis* (Figures 1, 4, and Supplemental Figure 6). MYB44 activates the expression of *MPK3* and *MPK6* by targeting their promoters, thus providing the molecular basis for protein production and phosphorylation (Figure 4 and Supplemental Figures 6 and 10). Phosphorylated MPK3 and MPK6 phosphorylate MYB44 in a functionally redundant manner, thereby enabling MYB44 to activate the expression of *MPK3*, *MPK6*, *EIN2*, and downstream defense responses (Figures 5 and 6). In particular, activation of *MPK3* and *MPK6* expression by MYB44 acts as a positive feedback regulatory mechanism for phosphorylation of MYB44 itself and both MAPKs (Figure 7). Through transcriptional and posttranscriptional regulation, MYB44, MPK3, and MPK6 constitute a functional cascade that effectively promotes PTI development (Figure 7). MPK4 may also have a role in this cascade, as it was slightly phosphorylated after flg22 treatment in the plants that carried a functional MYB44 (Figure 4); however, we do not have evidence to validate this hypothesis at present. PTI development also involves activation of *EIN2* transcription by MYB44 (Liu et al., 2011), and *EIN2* is required for *FLS2* expression (Figure 6), which is an essential step in PAMP recognition (Zipfel, et al., 2006; Zipfel, 2014) and PTI development (Singh et al., 2014; Sardar et al., 2017; Zhang et al., 2021; Figure 7). In summary,

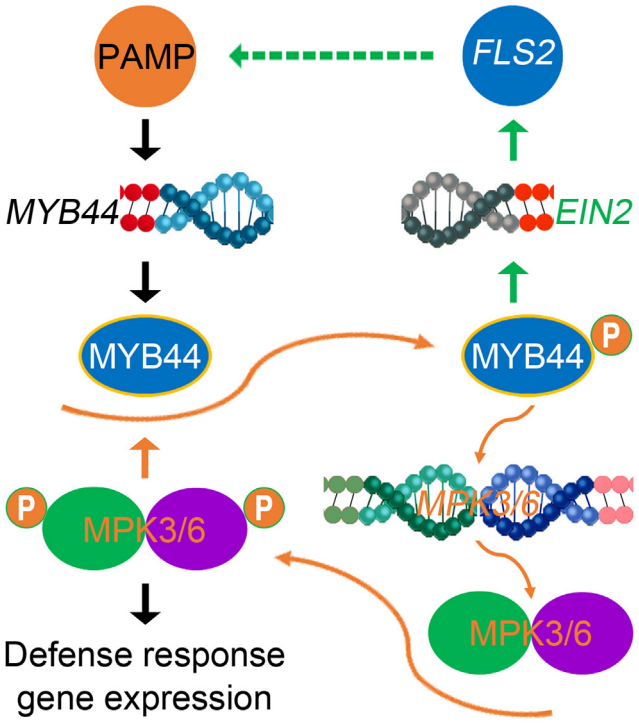

Figure 7. Model depicting the role of MYB44 in PTI regulation.
MYB44 regulates PTI by a main route (arrowheads in black) and an accessory route (arrowheads in green). In the former, a PAMP induces expression of *MYB44*, *MPK3*, and *MPK6*, leading to protein production. MYB44 binds to the promoters of *MPK3* and *MPK6* to activate their expression, thereby facilitating the phosphorylation of both kinases. Phosphorylated MPK3 and MPK6 function redundantly to phosphorylate MYB44, thus enabling it to activate *MPK3* and *MPK6* expression and further activate defense responses downstream of the PTI pathway (Figures 1–6). Transcriptional regulation by MYB44 and phosphorylation of MYB44 and both the MAPKs form a positive feedback regulatory loop (lines and arrowheads in orange) to intensify the defense responses. In the accessory route, defense responses are attributed to the role of MYB44 in activating *EIN2* transcription (Liu et al., 2011), which is required for *FLS2* expression, an essential step in PAMP recognition (Zipfel et al., 2006; Zipfel, 2014) and PTI development (Singh et al., 2014; Sardar et al., 2017; Zhang et al., 2021). Overall, MYB44 regulates the PTI pathway by promoting *EIN2* and *MPK3/6* expression.

MYB44 regulates the PTI pathway by promoting *EIN2* and *MPK3/6* expression (Figure 7).

This model is particularly focused on the function of MYB44 as an integral component of the PTI pathway and especially as an essential constituent of the MPK3/6 cascade (Figure 7). However, it omits information about the additional known activities of MPK3, MPK6, and MYB44 in plants. Functional multiplicity is a common characteristic of many PTI regulators, including MPK3 and MPK6. In addition to regulating PTI, MPK3 and MPK6 also regulate phytohormone-mediated basal resistance (Wang et al., 2018), mechanical damage–triggered immunity, and microbial effector–triggered immunity pathways (Ye et al., 2015). In addition to regulating the innate immunity systems, MPK3 and MPK6 also regulate growth and development (Li et al., 2017; Shao et al., 2020). Similarly, MYB44 has been demonstrated to have multiple effects in plants (Liu et al., 2010, 2011; Nguyen et al., 2012; Shim et al., 2012; Persak and Pitzschke, 2013; Qin et al., 2022; Zhao et al., 2022). MYB44 confers basal resistance through the salicylic acid signaling pathway (Zou et al., 2013) and is involved in crosstalk with phytohormone signaling (Jung et al., 2008; Hieno et al., 2016). MYB44 also enhances plant resistance against bacterial wilt by activating spermidine synthase (Qiu et al., 2019), suggesting a role for polyamines in MYB44-dependent immunity. Furthermore, MYB44 was implicated in a protein complex that suppresses a phosphatase involved in abscisic acid signaling (Nguyen and Cheong, 2018), which, however, often antagonizes disease resistance (de Torres Zabala et al., 2009). In addition, MYB44 contains a putative transcriptional repression (ethylene responsive element binding factor-associated amphiphilic repression) motif. This motif may have a suppressive effect on MYB44-mediated salinity tolerance, which can be impaired by adding an artificial ethylene responsive element binding factor-associated amphiphilic repression motif (LDLDL) to the C terminus of MYB44 (Persak and Pitzschke, 2014). Therefore, MYB44 participates in multiple immunity pathways by distinct mechanisms, among which the MPK3/6 cascade is merely responsible for MYB44-dependent PTI development that causes expression of defense response genes (Figure 7).

This model highlights the specific function of the MYB44–MPK3/6 cascade that is consistent with previous studies relating MYB44 to defense responses against pathogens (Zou et al., 2013), but it raises questions about possible existence of different mechanisms (Liu et al., 2011; Qiu et al., 2019). MPK3 and MPK6 are phosphorylated at basal levels in the *myb44* mutant (Figure 4C), suggesting possible roles of different TFs in MPK3 and MPK6 phosphorylation. This possibility cannot be excluded, especially because only 37 of the thousands of *Arabidopsis* TFs were tested in the present study. In addition to MYB44, three other TFs (MYB51, ZFP6, and RAP2.6) also affect PTI responses (Supplemental Figures 1 and 3); however, their mechanisms remain to be investigated. Furthermore, MYB44 may use different mechanisms to affect PTI. In *Arabidopsis* plants infested by the green peach aphid, MYB44 binds to the promoter of *EIN2* to activate its expression, thereby enhancing plant resistance against further infestation by the same insect (Liu et al., 2011). In *Arabidopsis* plants treated with flg22, EIN2 participates in MYB44-dependent PTI development at the stage of MPK3/6 phosphorylation and therefore affects downstream defense responses (Bethke et al., 2009; Boutrot et al., 2010; Mersmann et al., 2010; Tintor et al., 2013; Figure 6). In contrast to the WT *EIN2* gene, both of the *ein2* alleles—*ein2-1* and *ein2-5*—reduce, but do not eliminate, phosphorylation of MPK3 and MPK6 (Bethke et al., 2009; Boutrot et al., 2010; Figure 6), their phosphorylating activities (Bethke et al., 2009), *FSL2* gene expression (Tintor et al., 2013), and FLS2 protein production (Tintor et al., 2013). Thus, EIN2 contributes to a substantial part, rather than the full level, of PTI. In *Arabidopsis* plants treated with flg22, *EIN2* is required for expression of *FLS2* (Figure 6) and for ROS production and subsequent PTI responses to *Pst* infection (Mersmann et al., 2010; Figure 6). Thus, MYB44-dependent ROS generation (Figure 3) may be attributed to the role of MYB44 in *EIN2* activation (Mersmann et al., 2010; Figure 6) and the role of *EIN2*

in FLS2 signaling for ROS generation as well as MPK3 and MPK6 activation; however, this hypothesis requires verification in the future.

The multifaceted roles of MYB44 in defense and the multiple functions of MPK3 and MPK6 in development and immunity explain why the MYB44–MPK3/6 cascade (Figure 7) has not been characterized and why the knowledge gap between transcriptional and biochemical regulation of MAPKs has not been bridged until now. An apparent reason is the difficulty of performing detailed genetic analyses using stable transgenic and mutant plants because of the embryo lethality of the *mpk3/6* double mutant (Xu et al., 2014). Combined use of a conditional rescue strategy (Wang et al., 2007) and a chemical genetic approach has greatly accelerated dissection of MPK3 and MPK6 signaling in different immunity pathways (Ye et al., 2015). In the present study, we used the chemical genetic approach (Xu et al., 2014) to grow *mpk3/6* and *GVG:DD* plants so that the different versions of MYB44 could be introduced (Figures 5 and 6). This allowed us to elucidate the functional relationship between MYB44 and the MPK3/6 cascade and illustrate this relationship with a working model (Figure 7). The model highlights the transcriptional regulation of MPK3 and MPK6 by MYB44 and the phosphorylation of MYB44 by MPK3 and MPK6; however, it does not include the involvement of MYB44 in ROS generation (Figure 3).

PAMP-induced generation of an H_2O_2 signal in plant apoplasts and signal transport into plant cells are pivotal events in PTI signal transduction (Tian et al., 2016; Lu et al., 2022; Zhang et al., 2022), especially the MYB44–MPK3/6 cascade (Figure 3 and Supplemental Figure 8). Such a signal flux is consistent with previous demonstrations that PAMP-induced H_{2O2} generation in plant apoplasts and ensuing transport of the H_2O_2 signal into the cytosol facilitates PTI development and elicits downstream defense responses (Tian et al., 2016; Lu et al., 2022). H_2O_2 is generated in the apoplasts by the enzymatic activity of PM-associated RbohD when plants are infected by a pathogen or treated with a PAMP (Xu et al., 2014; Tian et al., 2016), and H_{2O2} is imported to the cytoplasm through aquaporin channels in the PM (Tian et al., 2016; Rodrigues et al., 2017; Zhang et al., 2022). However, subsequent steps, including how H_2O_2 joins the PTI pathway, have been unclear. Related studies (such as Segonzac et al., 2011; Xu et al., 2014; Tian et al., 2016 Rodrigues et al., 2017; Li et al., 2021; Lu et al., 2022; Zhang et al., 2022) support the notion that ROS production and MAPK activation are independent signaling branches; however, they simultaneously contribute to PAMP-induced resistance. In an *Arabidopsis* mutant lacking a functional RbohD, the PAMP-induced rapid ROS burst is completely blocked (Tian et al., 2016), but activation of the MPK3/6 cascade is unaffected (Xu et al., 2014; Tian et al., 2016). Indeed, the PAMP-induced RbohD-mediated ROS burst occurs similarly in the *mpk3*, *mpk6*, and *mpk3/6* mutants and in WT plants (Xu et al., 2014). Therefore, the rapid ROS burst and MPK3/6 activation are two early independent signaling events in PTI development. Moreover, H_2O_2 is not only involved in PTI but also participates in basal resistance, DTI, and effector-triggered immunity (Li et al., 2021). However, how H_2O_2 signaling is related to these distinct immunity pathways is an enduring question that remains to be answered.

MATERIALS AND METHODS

Plant materials and growth conditions

All *Arabidopsis* plants used in this study are in the Col-0 background. Seeds of TF-defective mutants were purchased from The Arabidopsis Information Resource (https://www.arabidopsis.org/). The mutants were characterized, *myb44/MYB44* and *MYB44OE* transgenic lines were generated and characterized (Liu et al., 2010; Zou et al., 2013), and all these plants were reproduced in the H.D. lab. Seeds of *mpk3*, *mpk6*, *mpk3/6*, and *GVG:DD* were provided by Professor Shuqun Zhang (University of Missouri). Seeds were incubated and plants were grown in 9-cm pots in plant growth chambers at 23°C ± 1°C with 8 h of illumination at 250 ± 50 μM quanta/m^2/s. In all experiments, 20-day-old uniform seedlings were used unless otherwise specified.

Plant treatments

The conditional *mpk3/6* double mutant carries an MPK6 variant (Wang et al., 2007) that has a defect at the ATP-binding site and therefore allows binding of amino-tert-butyl-naphthyl pyrazolo-pyrimidine (NA-PP1), an ATP analog that inhibits MPK6 phosphorylation (Xu et al., 2014). For this reason, treating conditional *mpk3/6* double mutant plants with NA-PP1 causes MPK6 to lose its phosphorylation activity in the mutant (Wang et al., 2007, Xu et al., 2014; Su et al., 2017). Therefore, NA-PP1 was used previously (Xu et al., 2014; Su et al., 2017) and in the present study to eliminate MPK6 phosphorylation activity in the conditional *mpk3/6* double mutant. In independent experiments, flg22 and ch8 were applied to all plant genotypes to induce PTI responses; DEX was used to treat *GVG:DD* plants to induce expression of $NtMEK2^{DD}$, thus triggering phosphorylation of both MPK3 and MPK6 (Wang et al., 2018); and NA-PP1 was applied to the conditional *mpk3/6* double mutant (Xu et al., 2014). Flg22, ch8, and DEX were prepared as 1-μM aqueous solutions amended with the surfactant Silwet L-77 at 0.03% v/v. An NA-PP1 stock solution of 1 mM was prepared with dimethyl sulfoxide (DMSO) by dissolving 4.5 mg NA-PP1 in 14.5 ml of DMSO, then diluted with pure water to 1 μM and amended with 0.03% v/v Silwet L-77 before use. Each solution was applied to plants by spraying over the plant tops using an atomizer. Similar treatment with an aqueous solution containing 0.03% v/v Silwet L-77 alone or both 0.03% Silwet L-77 and 14.5% DMSO (v/v) was used as an inactive control. Plants were treated as described above unless otherwise specified. Treated plants were subjected to different analyses according to the study purposes.

Bacterial infection assessment

Pst DC3000 inoculum was prepared as an aqueous bacterial suspension and adjusted to an optical density at 600 nm of 0.05 and a final $MgCl_2$ concentration of 10 mM. This inoculum and the mock control agent (10 mM $MgCl_2$) were amended with 0.03% v/v Silwet L-77 and applied to plants by spraying over the plant tops unless otherwise specified. The bacterial population in the leaves was determined at 3 dpi to assess the extent of infection. At 9 dpi, leaf chlorosis and necrosis symptoms were documented by photography, and disease severity was quantified as the ratio of lesion area to leaf area. Variations in leaf bacterial populations and symptom severity among different plant genotypes were used as criteria to evaluate the effects of different genes on immunity levels.

Gene expression analysis

All qRT-PCR experiments were performed with the QuantStudio3 Real-Time PCR System (Thermo Fisher Scientific), SYBR Premix-Ex Taq (TaKaRa), leaf RNA extracted using the TRIzol Total RNA Isolation Kit (TaKaRa), and specific primers (Supplemental Table 2). The expression level of each tested gene was determined by the $2^{-\Delta\Delta Ct}$ method relative to that of the constitutively expressed *EF1α* reference gene.

IB of plant proteins

Leaf protein extracts (Li et al., 2017) were separated by SDS–PAGE and blotted onto polyvinylidene fluoride membranes (Immobilon-p Transfer

membrane, Millipore) in a semi-dry transfer cell (Trans-Blot SD, Bio-Rad). MYB44 and MYB44-His were detected by hybridization with specific α-MYB44 antibodies prepared by immunizing Dutch white rabbits and α-His (Beyotime Biotech), respectively (Figure 2H). MPK3 and MPK6 were detected by hybridization with the specific α-MAPK antibody (Phospho-p44/42 MAPK Erk1/2 Thr202/Tyr204 D13.14.4E XP Rabbit mAb, Cell Signaling Technology, Shanghai, China; Figures 1B, 4C, 5D, 6D, and 6E). MPK3 and MPK6 were also detected by specific α-MPK3 and α-MPK6 antibodies (PHYTOAB, San Jose, CA, USA) (Figures 1D, 4C, 5D, and 6D). The IB signals were captured with an automatic imaging system (ChemiScope series, Clinx Science Instruments).

Gene modification

Site-directed mutation was applied to the *MYB44* nucleotide sequence at sites 157 and 433 to change both codes for serine to L-aspartic acid (D) and L-alanine (A), yielding the *MYB44* gene mutants $MYB44^{DD}$ and $MYB44^{AA}$, respectively. $MYB44^{DD}$ and $MYB44^{AA}$ were fused separately to a $his_{(6)}$-tag by RT-PCR using leaf RNA and specific primer pairs in which the downstream primer was linked with $his_{(6)}$ (Supplemental Table 2), yielding the recombinant genes $MYB44^{DD}$-*his* and $MYB44^{AA}$-*his*. $MYB44^{DD}$-*his* and $MYB44^{AA}$-*his* were inserted separately into the plant binary vector pCAMBIA1300 (Liu et al., 2011). Subsequently, each of the recombinant vectors was used to transform the *myb44* mutant for ChIP assays (Figure 4E).

Site-directed mutation was also applied to the *MKK5* nucleotide sequence at sites 643 and 661 to change both codes for threonine and serine to L-aspartic acid, yielding the gene mutant $MKK5^{DD}$ (Li et al., 2017). The *GST-*$MKK5^{DD}$ fusion gene was generated by ligating both sequences generated by overlapping PCR and cloned into the pET32(a) prokaryotic expression vector. The recombinant vector was used for prokaryotic production of the GST-$MKK5^{DD}$ fusion protein for use in phosphorylation assays (Figure 5C).

The HA coding sequence containing 27 nucleotides was added to the 3′-terminal end of *MPK3* and *MPK6* by RT-PCR using leaf RNA and specific primer pairs in which the downstream primer was linked with the HA code (Supplemental Table 2). A similar method was used for MYB44 fusion to $his_{(6)}$. The *MPK3-HA*, *MPK6-HA*, *MYB44-his*, and $MYB44^{AA}$-*his* fusion genes were individually inserted into pET32(a), followed by prokaryotic production of the fusion proteins for use in *in vitro* phosphorylation assays (Figure 5C). In independent experiments, *MPK3-HA* and *MPK6-HA* were inserted separately into pCAMBIA1300, and each of the resulting recombinant vectors was transferred into *myb44*/*MYB44-his#2* seedlings; *in vivo* phosphorylation assays were performed 48 h after plant transformation (Figure 5D).

Protein phosphorylation analysis

The *in vitro* and *in vivo* phosphorylation assays were performed using the Phos-tag reagent kit (NARD Institute) and its companion protocol. For the *in vitro* assay (Figure 5C), the tested proteins were fused to an HA, GST, or His tag as described above; the fusion proteins were produced by prokaryotic expression and purified by affinity chromatography using the corresponding resins. Protein concentrations were quantified using a BCA kit (Beijing Solarbio Technology, Beijing). A total of 0.2 mg of purified MPK3-HA or MPK6-HA protein was activated by incubation with 0.05 mg of purified GST-$MKK5^{DD}$ in the reaction buffer at 30°C for 30 min. The reaction buffer consisted of 20 mM Tris–HCl (pH 7.5), 10 mM $MgCl_2$, 50 mM ATP, and 1 mM DTT dissolved in pure water. With the same buffer and incubation conditions, activated MPK3 or MPK6 was used to phosphorylate MYB44-His or $MYB44^{AA}$-His fusion protein at a 1:10 ratio. The phosphorylation reaction was stopped by addition of 6× protein loading buffer. For the *in vivo* assay (Figure 5B and 5D), MYB44-His phosphorylated *in planta* was detected by the Phos-tag α-His IB technique. In brief, the technique involved protein electrophoresis in a 12% SDS–PAGE gel amended with 50 mM Phos-tag and 100 mM $MnCl_2$, protein blotting onto polyvinylidene fluoride membranes, hybridization with α-His, and automatic documentation of the hybridization signals.

Callose visualization

Callose deposition on leaf surfaces of flg22-treated and water-treated (control) plants was observed 45 min after treatment. Callose deposition was visualized as a violet color after staining the leaves with aniline blue (Tian et al., 2016). The relative level of callose deposition was quantified as the number of callose deposition sites per leaf.

Whole-plant ROS live imaging

ROS live imaging with intact plants was performed using a previously described protocol (Matsuo et al., 2015). The ROS-probing dye H_2DCFDA (Millipore-Sigma) was prepared as a 50 μM aqueous solution in 50 mM phosphate buffer (pH 7.4) and amended with 0.03% v/v Silwet L-77 (Tian et al., 2016). Plants were treated with this solution by spraying over the tops, then maintained in the dark for 30 min. The dye-treated and etiolated plants were further treated with pure water or an aqueous solution containing 0.03% Silwet L-77 or both 0.03% Silwet L-77 and 1 μM flg22. The plants were observed immediately and then at 5-min intervals over the next 45 min. Images were acquired on an IVIS Lumina S2 platform using Living Image 3.1 software in acquisition mode (PerkinElmer, Waltham, MA, USA) via a constant image set at excitation/emission 500 nm, F 1, 1-s exposure, and medium binning.

Luc imaging

Recombinant genes (Luc^C-*MYB44*, Luc^N-*MPK3*, Luc^N-*MPK6*) were inserted into the *P35S:*Luc^N or *P35S:*Luc^C vector (Zhou et al., 2018). Each recombinant vector was transferred into cells of *Agrobacterium tumefaciens* strain GV3101. A suspension mixture of recombinant bacteria carrying Luc^N and Luc^C alone or fused to one of the tested proteins was infiltrated into the intercellular spaces of tobacco (*Nicotiana benthamiana*) or *Arabidopsis* leaves. Two days later, leaves were observed with an *in vivo* imaging system (Zhou et al., 2018). *Arabidopsis* plants were grown as described above, and tobacco plants were grown similarly but at 25°C ± 1°C.

ChIP PCR and ChIP qPCR analyses

The EpiQuik Plant ChIP Kit (Epigentek) and its accompanying instructions were used for ChIP experiments performed on the *myb44*-complemented transgenic line *myb44*/*MYB44-his*#2 and *myb44* mutant seedlings transformed with $MYB44^{DD}$-*his* and $MYB44^{AA}$-*his*. With tightly scheduled operation steps, the experiments began with incubation of antibodies, including α-His used to precipitate DNA fragments from chromatin and the non-immune protein immunoglobulin G (IgG) used as an antibody-free control. The α-His or IgG protein was incubated with antibody buffer solution in the provided assay strips at room temperature for 2 h. During this period, chromatin was isolated from plant leaves.

To extract plant chromatin, a 30-ml aqueous solution of 1% v/v formaldehyde was poured into a 50-ml plastic tube, and excised leaves were added to the tube. The tube was immediately vacuumed with a pump for 10 min, and gas was then released back into the tube to allow sufficient crosslinking between the plant tissues and the formaldehyde. Approximately 1 min later, the crosslinking reaction was stopped by adding 300 μl of 0.125 M glycine into the formaldehyde solution in the tube, followed by vacuum infiltration for 5 min and gas flow back into the tube one more time. The formaldehyde-linked leaves were removed from the tube, wiped with clear tissue papers to remove surface water, and ground into powder with a mortar and pestle. The leaf powder was transferred to another 50-ml plastic tube and suspended in 20 ml of lysis buffer solution, then centrifuged at 4°C and 14 000 rpm for 45 min. The supernatant was removed, and the chromatin pellet was resuspended in 300 μl of the same lysis buffer in a 1.5-ml plastic tube. The chromatin was fragmented by

sonication at moderate power for 10 min to produce 200–500 bp DNA fragments in the supernatant.

This supernatant was divided into three groups for PCR. In the first group, the supernatant was used directly as input for the PCR analysis. In the second group, DNA fragments in the supernatant were subjected to immunoprecipitation. In brief, 100 μl of the supernatant was mixed with an α-His antibody buffer solution already incubated in the assay strip, incubated at room temperature for 90 min, and then centrifuged as above. The final supernatant (containing α-His and the DNA fragment mixture) was transferred to a resin spin column and eluted with elution buffer to yield purified DNA fragments. In the third group, the operations performed with α-His antibody buffer solution were performed with buffer solution that contained the IgG protein. PCR was performed with pairs of primers specific to the *MPK3* or *MPK6* promoters and CDSs (Supplemental Table 2). Each pair of primers was used in combination with the DNA template from the input (in the first group) or from the DNA samples precipitated with α-His (in the second group), or in combination with the eluate from the mixture of IgG and chromatin fragments (in the third group).

The ChIP qPCR analysis was performed using a standard protocol (Kim and Dekker, 2015). Each of the supernatants containing immunoprecipitated DNA was amplified by qPCR performed with primers specific to the *MAPK* promoter (Supplemental Table 2). Enrichment fold of the promoter through amplification by ChIP qPCR was used to quantify the protein–DNA interaction. Enrichment fold was determined as described previously (Kim and Dekker, 2015).

Statistical analysis

Quantitative data were subjected to Student's *t*-tests or analysis of variance and Duncan's new multiple range tests using GraphPad Prism 8.0 (https://www.graphpad.com/). Numbers of experimental repeats are specified in the figure legends.

ACCESSION NUMBERS

Accession numbers of genes analyzed in this study are provided in Supplemental Table 2.

DATA AVAILABILITY

The data supporting the results are available in the supplemental information files.

SUPPLEMENTAL INFORMATION

Supplemental information is available at *Plant Communications Online*.

FUNDING

This study was supported by the Natural Science Foundation of China (grant numbers 31772247, 32072399, and 32170202) and the Natural Science Foundation of Shandong Province (grant numbers ZR2020MC113, ZR2020MC120, and ZR2020QC126).

AUTHOR CONTRIBUTIONS

Z.W., X.L., and X.Y. performed the experiments, analyzed the data, and wrote the paper. J.M., K.L., Y.A., Z.S., Q.W., M.Z., L.Q., L.Z., S.Z., L.C., and C.S. performed the experiments. H.D., M.Z., and X.C. designed the experiments and wrote the paper. H.D. conceived the study and finalized the paper.

ACKNOWLEDGMENTS

We thank Dr. Shuqun Zhang (University of Missouri) for the gift of *mapk* and *GVG:DD* seeds. We thank former students Dr. Ruoxue Liu (Nanjing Normal University) and Dr. Beibei Lü (Shanghai Academy of Agricultural Sciences) for characterizing the *myb44/MYB44* and *MYB44*OE progenies. No conflict of interest is declared.

Received: October 13, 2022
Revised: April 3, 2023
Accepted: May 18, 2023
Published: May 22, 2023

REFERENCES

Adachi, H., Nakano, T., Miyagawa, N., Ishihama, N., Yoshioka, M., Katou, Y., Yaeno, T., Shirasu, K., and Yoshioka, H. (2015). WRKY transcription factors phosphorylated by MAPK regulate a plant immune NADPH oxidase in *Nicotiana benthamiana*. Plant Cell **27**:2645–2663.

Alonso, J.M., Hirayama, T., Roman, G., Nourizadeh, S., and Ecker, J.R. (1999). EIN2, a bifunctional transducer of ethylene and stress responses in *Arabidopsis*. Science **284**:2148–2152.

Asai, T., Tena, G., Plotnikova, J., Willmann, M.R., Chiu, W.L., Gomez-Gomez, L., Boller, T., Ausubel, F.M., and Sheen, J. (2002). MAP kinase signalling cascade in *Arabidopsis* innate immunity. Nature **415**:977–983.

Bethke, G., Scheel, D., Lee, J., Pöschl, Y., Gust, A.A., Scheel, D., and Lee, J. (2009). Flg22 regulates the release of an ethylene response factor substrate from MAP kinase 6 in *Arabidopsis thaliana* via ethylene signaling. Plant Signal. Behav. **4**:672–674.

Bigeard, J., Colcombet, J., and Hirt, H. (2015). Signaling mechanisms in pattern-triggered immunity (PTI). Mol. Plant **8**:521–539.

Bi, G., Zhou, Z., Wang, W., Li, L., Rao, S., Wu, Y., Zhang, X., Menke, F.L.H., Chen, S., and Zhou, J.M. (2018). Receptor-like cytoplasmic kinases directly link diverse pattern recognition receptors to the activation of mitogen-activated protein kinase cascades in Arabidopsis. Plant Cell **30**:1543–1561.

Birkenbihl, R.P., Kracher, B., Ross, A., Kramer, K., Finkemeier, I., and Somssich, I.E. (2018). Principles and characteristics of the Arabidopsis WRKY regulatory network during early MAMP-triggered immunity. Plant J. **96**:487–502.

Boutrot, F., Segonzac, C., Chang, K.N., Qiao, H., Ecker, J.R., Zipfel, C., and Rathjen, J.P. (2010). Direct transcriptional control of the *Arabidopsis* immune receptor FLS2 by the ethylene-dependent transcription factors EIN3 and EIL1. Proc. Natl. Acad. Sci. USA **107**:14502–14507.

Chen, X., Ma, J., Wang, X., Lu, K., Liu, Y., Zhang, L., Peng, J., Chen, L., Yang, M., Li, Y., et al. (2021). Functional modulation of an aquaporin to intensify photosynthesis and abrogate bacterial virulence in rice. Plant J. **108**:330–346.

Clay, N.K., Adio, A.M., Denoux, C., Jander, G., and Ausubel, F.M. (2009). Glucosinolate metabolites required for an *Arabidopsis* innate immune response. Science **323**:95–101.

de Torres-Zabala, M., Bennett, M.H., Truman, W.H., and Grant, M.R. (2009). Antagonism between salicylic and abscisic acid reflects early host-pathogen conflict and moulds plant defence responses. Plant J. **59**:375–386.

Dunning, F.M., Sun, W., Jansen, K.L., Helft, L., and Bent, A.F. (2007). Identification and mutational analysis of Arabidopsis FLS2 leucine-rich repeat domain residues that contribute to flagellin perception. Plant Cell **19**:3297–3313.

Gómez-Gómez, L., and Boller, T. (2000). FLS2: an LRR receptor-like kinase involved in the perception of the bacterial elicitor flagellin in *Arabidopsis*. Mol. Cell **5**:1003–1011.

Hieno, A., Naznin, H.A., Hyakumachi, M., Higuchi-Takeuchi, M., Matsui, M., and Yamamoto, Y.Y. (2016). Possible involvement of MYB44-mediated stomatal regulation in systemic resistance induced

by *Penicillium simplicissimum* GP17-2 in *Arabidopsis*. Microb. Environ. **31**:154–159.

Huang, P.Y., Zhang, J., Jiang, B., Chan, C., Yu, J.H., Lu, Y.P., Chung, K., and Zimmerli, L. (2019). NINJA-associated ERF19 negatively regulates Arabidopsis pattern-triggered immunity. J. Exp. Bot. **70**:1033–1047.

Jung, C., Seo, J.S., Han, S.W., Koo, Y.J., Kim, C.H., Song, S.I., Nahm, B.H., Choi, Y.D., and Cheong, J.J. (2008). Overexpression of *AtMYB44* enhances stomatal closure to confer abiotic stress tolerance in transgenic Arabidopsis. Plant Physiol. (Wash. D C) **146**:623–635.

Kang, S., Yang, F., Li, L., Chen, H., Chen, S., and Zhang, J. (2015). The Arabidopsis transcription factor BRASSINOSTEROID INSENSITIVE1-ETHYL METHANESULFONATE-SUPPRESSOR1 is a direct substrate of MITOGEN-ACTIVATED PROTEIN KINASE6 and regulates immunity. Plant Physiol. (Wash. D C) **167**:1076–1086.

Kanyuka, K., and Rudd, J.J. (2019). Cell surface immune receptors: the guardians of the plant's extracellular spaces. Curr. Opin. Plant Biol. **50**:1–8.

Kim, T.H., and Dekker, J. (2015). ChIP-quantitative polymerase chain reaction (ChIP-qPCR). Cold Spring Harb. Protoc. **2018**. pdb.prot082628.

Li, B., Jiang, S., Yu, X., Cheng, C., Chen, S., Cheng, Y., Yuan, J.S., Jiang, D., He, P., and Shan, L. (2015). Phosphorylation of antihelix transcriptional repressor ASR3 by MAP KINASE4 negatively regulates Arabidopsis immunity. Plant Cell **27**:839–856.

Li, B., Meng, X., Shan, L., and He, P. (2016). Transcriptional regulation of pattern-triggered immunity in plants. Cell Host Microbe **19**:641–650.

Li, H., Ding, Y., Shi, Y., Zhang, X., Zhang, S., Gong, Z., and Yang, S. (2017). MPK3- and MPK6-mediated ICE1 phosphorylation negatively regulates ICE1 stability and freezing tolerance in *Arabidopsis*. Dev. Cell **43**:630–642.e4.

Li, P., Zhao, L., Qi, F., Htwe, N.M.P.S., Li, Q., Zhang, D., Lin, F., Shang-Guan, K., and Liang, Y. (2021). The receptor-like cytoplasmic kinase RIPK regulates broad-spectrum ROS signaling in multiple layers of plant immune system. Mol. Plant **14**:1652–1667.

Liu, R., Chen, L., Jia, Z., Lü, B., Shi, H., Shao, W., and Dong, H. (2011). Transcription factor AtMYB44 regulates induced expression of the *ETHYLENE INSENSITIVE2* gene in *Arabidopsis* responding to a harpin protein. Mol. Plant Microbe Interact. **24**:377–389.

Liu, R., Lü, B., Wang, X., Zhang, C., Zhang, S., Qian, J., Chen, L., Shi, H., and Dong, H. (2010). Thirty-seven transcription factor genes differentially respond to a harpin protein and affect resistance to the green peach aphid in. J. Biosci. **35**:435–450.

Liu, Y., Leary, E., Saffaf, O., Frank Baker, R., and Zhang, S. (2022). Overlapping functions of YDA and MAPKKK3/MAPKKK5 upstream of MPK3/MPK6 in plant immunity and growth/development. J. Integr. Plant Biol. **64**:1531–1542.

Logemann, E., Birkenbihl, R.P., Rawat, V., Schneeberger, K., Schmelzer, E., and Somssich, I.E. (2013). Functional dissection of the *PROPEP2* and *PROPEP3* promoters reveals the importance of WRKY factors in mediating microbe-associated molecular pattern-induced expression. New Phytol. **198**:1165–1177.

Lü, B., Sun, W., Zhang, S., Zhang, C., Qian, J., Wang, X., Gao, R., and Dong, H. (2011). $HrpN_{Ea}$-induced deterrent effect on phloem feeding of the green peach aphid *Myzus persicae* requires *AtGSL5* and *AtMYB44* genes in *Arabidopsis thaliana*. J. Biosci. **36**:123–137.

Lu, K., Chen, X., Yao, X., An, Y., Wang, X., Qin, L., Li, X., Wang, Z., Liu, S., Sun, Z., et al. (2022). Phosphorylation of a wheat aquaporin at two sites enhances both plant growth and defense. Mol. Plant **15**:1772–1789.

Luna, E., Pastor, V., Robert, J., Flors, V., Mauch-Mani, B., and Ton, J. (2011). Callose deposition: a multifaceted plant defense response. Mol. Plant Microbe Interact. **24**:183–193.

Matsuo, M., Johnson, J.M., Hieno, A., Tokizawa, M., Nomoto, M., Tada, Y., Godfrey, R., Obokata, J., Sherameti, I., Yamamoto, Y.Y., et al. (2015). High REDOX RESPONSIVE TRANSCRIPTION FACTOR1 levels result in accumulation of reactive oxygen species in *Arabidopsis thaliana* shoots and roots. Mol. Plant **8**:1253–1273.

Meng, X., Xu, J., He, Y., Yang, K.Y., Mordorski, B., Liu, Y., and Zhang, S. (2013). Phosphorylation of an ERF transcription factor by Arabidopsis MPK3/MPK6 regulates plant defense gene induction and fungal resistance. Plant Cell **25**:1126–1142.

Mersmann, S., Bourdais, G., Rietz, S., and Robatzek, S. (2010). Ethylene signaling regulates accumulation of the FLS2 receptor and is required for the oxidative burst contributing to plant immunity. Plant Physiol. (Wash. D C) **154**:391–400.

Nagy, Z., Comer, S., and Smolenski, A. (2018). Analysis of protein phosphorylation using Phos-tag gels. Curr. Protoc. Protein Sci. **93**:e64.

Ngou, B.P.M., Ahn, H.K., Ding, P., and Jones, J.D.G. (2021). Mutual potentiation of plant immunity by cell-surface and intracellular receptors. Nature **592**:110–115.

Nguyen, N.H., and Cheong, J.J. (2018). AtMYB44 interacts with TOPLESS-RELATED corepressors to suppress *protein phosphatase 2C* gene transcription. Biochem. Biophys. Res. Commun. **507**:437–442.

Nguyen, X.C., Hoang, M.H.T., Kim, H.S., Lee, K., Liu, X.M., Kim, S.H., Bahk, S., Park, H.C., and Chung, W.S. (2012). Phosphorylation of the transcriptional regulator MYB44 by mitogen activated protein kinase regulates *Arabidopsis* seed germination. Biochem. Biophys. Res. Commun. **423**:703–708.

Offor, B.C., Dubery, I.A., and Piater, L.A. (2020). Prospects of gene knockouts in the functional study of MAMP-triggered immunity: a review. Int. J. Mol. Sci. **21**:2540.

Persak, H., and Pitzschke, A. (2013). Tight interconnection and multi-level control of *Arabidopsis* MYB44 in MAPK cascade signalling. PLoS One **8**, e57547.

Persak, H., and Pitzschke, A. (2014). Dominant repression by Arabidopsis transcription factor MYB44 causes oxidative damage and hypersensitivity to abiotic stress. Int. J. Mol. Sci. **15**:2517–2537.

Pitzschke, A., Djamei, A., Teige, M., and Hirt, H. (2009). VIP1 response elements mediate mitogen-activated protein kinase 3-induced stress gene expression. Proc. Natl. Acad. Sci. USA **106**:18414–18419.

Qin, B., Fan, S.L., Yu, H.Y., Lu, Y.X., and Wang, L.F. (2022). HbMYB44, a rubber tree MYB transcription factor with versatile functions in modulating multiple phytohormone signaling and abiotic stress responses. Front. Plant Sci. **13**. 893896–896.

Qiu, Z., Yan, S., Xia, B., Jiang, J., Yu, B., Lei, J., Chen, C., Chen, L., Yang, Y., Wang, Y., et al. (2019). The eggplant transcription factor MYB44 enhances resistance to bacterial wilt by activating the expression of spermidine synthase. J. Exp. Bot. **70**:5343–5354.

Rasmussen, M.W., Roux, M., Petersen, M., and Mundy, J. (2012). MAP kinase cascades in Arabidopsis innate immunity. Front. Plant Sci. **3**:169.

Ren, D., Liu, Y., Yang, K.Y., Han, L., Mao, G., Glazebrook, J., and Zhang, S. (2008). A fungal-responsive MAPK cascade regulates phytoalexin biosynthesis in *Arabidopsis*. Proc. Natl. Acad. Sci. USA **105**:5638–5643.

Rodrigues, O., Reshetnyak, G., Grondin, A., Saijo, Y., Leonhardt, N., Maurel, C., and Verdoucq, L. (2017). Aquaporins facilitate hydrogen peroxide entry into guard cells to mediate ABA- and pathogen-triggered stomatal closure. Proc. Natl. Acad. Sci. USA **114**:9200–9205.

Sardar, A., Nandi, A.K., and Chattopadhyay, D. (2017). CBL-interacting protein kinase 6 negatively regulates immune response to *Pseudomonas syringae* in Arabidopsis. J. Exp. Bot. **68**:3573–3584.

Schulze, S., Yu, L., Hua, C., Zhang, L., Kolb, D., Weber, H., Ehinger, A., Saile, S.C., Stahl, M., Franz-Wachtel, M., et al. (2022). The *Arabidopsis* TIR-NBS-LRR protein CSA1 guards BAK1-BIR3 homeostasis and mediates convergence of pattern- and effector-induced immune responses. Cell Host Microbe **30**:1717–1731.e6.

Segonzac, C., Feike, D., Gimenez-Ibanez, S., Hann, D.R., Zipfel, C., and Rathjen, J.P. (2011). Hierarchy and roles of pathogen-associated molecular pattern-induced responses in *Nicotiana benthamiana*. Plant Physiol. (Wash. D C) **156**:687–699.

Serpa, V., Vernal, J., Lamattina, L., Grotewold, E., Cassia, R., and Terenzi, H. (2007). Inhibition of AtMYB2 DNA-binding by nitric oxide involves cysteine S-nitrosylation. Biochem. Biophys. Res. Commun. **361**:1048–1053.

Shao, Y., Yu, X., Xu, X., Li, Y., Yuan, W., Xu, Y., Mao, C., Zhang, S., and Xu, J. (2020). The YDA-MKK4/MKK5-MPK3/MPK6 cascade functions downstream of the RGF1-RGI ligand-receptor pair in regulating mitotic activity in root apical meristem. Mol. Plant **13**:1608–1623.

Shim, J.S., Jung, C., Lee, S., Min, K., Lee, Y.W., Choi, Y., Lee, J.S., Song, J.T., Kim, J.K., and Choi, Y.D. (2012). AtMYB44 regulates WRKY70 expression and modulates antagonistic interaction between salicylic acid and jasmonic acid signaling. Plant J. **73**:483–495.

Singh, P., Yekondi, S., Chen, P.W., Tsai, C.H., Yu, C.W., Wu, K., and Zimmerli, L. (2014). Environmental history modulates Arabidopsis pattern-triggered immunity in a HISTONE ACETYLTRANSFERASE1-dependent manner. Plant Cell **26**:2676–2688.

Sun, T., Nitta, Y., Zhang, Q., Wu, D., Tian, H., Lee, J.S., and Zhang, Y. (2018). Antagonistic interactions between two MAP kinase cascades in plant development and immune signaling. EMBO Rep. **19**, e45324.

Thara, V.K., Tang, X., Gu, Y.Q., Martin, G.B., and Zhou, J.M. (1999). *Pseudomonas syringae* pv *tomato* induces the expression of tomato EREBP-like genes *PTI4* and *PTI5* independent of ethylene, salicylate and jasmonate. Plant J. **20**:475–483.

Tian, H., Wu, Z., Chen, S., Ao, K., Huang, W., Yaghmaiean, H., Sun, T., Xu, F., Zhang, Y., Wang, S., et al. (2021). Activation of TIR signalling boosts pattern-triggered immunity. Nature **598**:500–503.

Tian, S., Wang, X., Li, P., Wang, H., Ji, H., Xie, J., Qiu, Q., Shen, D., and Dong, H. (2016). Plant aquaporin AtPIP1;4 links apoplastic H_2O_2 induction to disease immunity pathways. Plant Physiol. **171**:1635–1650.

Tintor, N., Ross, A., Kanehara, K., Yamada, K., Fan, L., Kemmerling, B., Nürnberger, T., Tsuda, K., and Saijo, Y. (2013). Layered pattern receptor signaling via ethylene and endogenous elicitor peptides during *Arabidopsis* immunity to bacterial infection. Proc. Natl. Acad. Sci. USA **110**:6211–6216.

Tsuda, K., and Somssich, I.E. (2015). Transcriptional networks in plant immunity. New Phytol. **206**:932–947.

Wang, D., Chai, G., Xu, L., Yang, K., Zhuang, Y., Yang, A., Liu, S., Kong, Y., and Zhou, G. (2022). Phosphorylation-mediated inactivation of C3H14 by MPK4 enhances bacterial-triggered immunity in Arabidopsis. Plant Physiol. **190**:1941–1959.

Wang, H., Ngwenyama, N., Liu, Y., Walker, J.C., and Zhang, S. (2007). Stomatal development and patterning are regulated by environmentally responsive mitogen-activated protein kinases in Arabidopsis. Plant Cell **19**:63–73.

Wang, Y., Schuck, S., Wu, J., Yang, P., Döring, A.C., Zeier, J., and Tsuda, K. (2018). MPK3/6-WRKY33-ALD1-pipecolic acid regulatory loop contributes to systemic acquired resistance. Plant Cell **30**:2480–2494.

Wu, Z., Han, S., Zhou, H., Tuang, Z.K., Wang, Y., Jin, Y., Shi, H., and Yang, W. (2019). Cold stress activates disease resistance in *Arabidopsis thaliana* through a salicylic acid dependent pathway. Plant Cell Environ. **42**:2645–2663.

Xu, G., Greene, G.H., Yoo, H., Liu, L., Marqués, J., Motley, J., and Dong, X. (2017). Global translational reprogramming is a fundamental layer of immune regulation in plants. Nature **545**:487–490.

Xu, J., Meng, J., Meng, X., Zhao, Y., Liu, J., Sun, T., Liu, Y., Wang, Q., and Zhang, S. (2016). Pathogen-responsive MPK3 and MPK6 reprogram the biosynthesis of indole glucosinolates and their derivatives in Arabidopsis immunity. Plant Cell **28**:1144–1162.

Xu, J., Xie, J., Yan, C., Zou, X., Ren, D., and Zhang, S. (2014). A chemical genetic approach demonstrates that MPK3/MPK6 activation and NADPH oxidase-mediated oxidative burst are two independent signaling events in plant immunity. Plant J. **77**:222–234.

Ye, L., Li, L., Wang, L., Wang, S., Li, S., Du, J., Zhang, S., and Shou, H. (2015). MPK3/MPK6 are involved in iron deficiency-induced ethylene production in *Arabidopsis*. Front. Plant Sci. **6**:953.

Yoo, H., Greene, G.H., Yuan, M., Xu, G., Burton, D., Liu, L., Marqués, J., and Dong, X. (2020). Translational regulation of metabolic dynamics during effector-triggered immunity. Mol. Plant **13**:88–98.

Yuan, M., Ngou, B.P.M., Ding, P., and Xin, X.F. (2021). PTI-ETI crosstalk: an integrative view of plant immunity. Curr. Opin. Plant Biol. **62**, 102030.

Zhang, H., Hong, Y., Huang, L., Li, D., and Song, F. (2016). *Arabidopsis* AtERF014 acts as a dual regulator that differentially modulates immunity against *Pseudomonas syringae* pv. *tomato* and *Botrytis cinerea*. Sci. Rep. **6**, 30251.

Zhang, J., and Zhou, J.M. (2010). Plant immunity triggered by microbial molecular signatures. Mol. Plant **3**:783–793.

Zhang, J., Coaker, G., Zhou, J.M., and Dong, X. (2020). Plant immune mechanisms: from reductionistic to holistic points of view. Mol. Plant **13**:1358–1378.

Zhang, M., Shi, H., Li, N., Wei, N., Tian, Y., Peng, J., Chen, X., Zhang, L., Zhang, M., and Dong, H. (2022). Aquaporin OsPIP2;2 links the H_2O_2 signal and a membrane-anchored transcription factor to promote plant defense. Plant Physiol. (Wash. D C) **188**:2325–2341.

Zhang, T.Y., Li, Z.Q., Zhao, Y.D., Shen, W.J., Chen, M.S., Gao, H.Q., Ge, X.M., Wang, H.Q., Li, X., and He, J.M. (2021). Ethylene-induced stomatal closure is mediated via MKK1/3-MPK3/6 cascade to EIN2 and EIN3. J. Integr. Plant Biol. **63**:1324–1340.

Zhao, B., Shao, Z., Wang, L., Zhang, F., Chakravarty, D., Zong, W., Dong, J., Song, L., and Qiao, H. (2022). MYB44-ENAP1/2 restricts HDT4 to regulate drought tolerance in *Arabidopsis*. PLoS Genet. **18**, e1010473.

Zhou, Z., Bi, G., and Zhou, J.M. (2018). Luciferase complementation assay for protein-protein interactions in plants. Curr. Opin. Plant Biol. **3**:42–50.

Zipfel, C. (2014). Plant pattern-recognition receptors. Trends Immunol. **35**:345–351.

Zipfel, C., Kunze, G., Chinchilla, D., Caniard, A., Jones, J.D.G., Boller, T., and Felix, G. (2006). Perception of the bacterial PAMP EF-Tu by the receptor EFR restricts *Agrobacterium*-mediated transformation. Cell **125**:749–760.

Zipfel, C., Robatzek, S., Navarro, L., Oakeley, E.J., Jones, J.D.G., Felix, G., and Boller, T. (2004). Bacterial disease resistance in *Arabidopsis* through flagellin perception. Nature **428**:764–767.

Zou, B., Jia, Z., Tian, S., Wang, X., Gou, Z., Lü, B., and Dong, H. (2013). AtMYB44 positively modulates disease resistance to *Pseudomonas syringae* through the salicylic acid signalling pathway in *Arabidopsis*. Funct. Plant Biol. **40**:304–313.